

Classification and characterization using HCT/HFOSC spectra of carbon stars selected from the HES survey

Meenakshi Purandardas^{1,2*} and Aruna Goswami¹

^{1*}Indian Institute of Astrophysics, , Koramangala, , Bangalore, 560034,
Karnataka, India.

^{2*}Department of Physics and Electronics, CHRIST (Deemed to be
University), Bangalore, 560029, Karnataka, India.

*Corresponding author(s). E-mail(s): meenakshi.p@christuniversity.in;
Contributing authors: aruna@iiap.res.in;

Abstract

We present results from the analysis of 88 carbon stars selected from Hamburg/ESO (HES) survey using low-resolution spectra ($R \sim 1330$ & 2190). The spectra were obtained with the Himalayan Faint Object Spectrograph Camera (HFOSC) attached to the 2-m Himalayan Chandra Telescope (HCT). Using a well-defined spectral criteria based on the strength of carbon molecular bands, the stars are classified into different groups. In our sample, we have identified 53 CH stars, four C-R stars, and two C-N type stars. Twenty-nine stars could not be classified due to the absence of prominent C_2 molecular bands in their spectra. We could derive the atmospheric parameters for 36 stars. The surface temperature is determined using photometric calibrations and synthesis of the H-alpha line profile. The surface gravity $\log g$ estimates are obtained using parallax estimates from the Gaia DR3 database whenever possible. Microturbulent velocity (ζ) is derived using calibration equation of $\log g$ & ζ . We could determine metallicity for 48 objects from near-infrared Ca II triplet features using calibration equations. The derived metallicity ranges from $-0.43 \leq [Fe/H] \leq -3.49$. Nineteen objects are found to be metal-poor ($[Fe/H] \leq -1$), 14 very metal-poor ($[Fe/H] \leq -2$), and five extremely metal-poor ($[Fe/H] \leq -3.0$) stars. Eleven objects are found to have a metallicity in the range $-0.43 \leq [Fe/H] \leq -0.97$. We could derive the carbon abundance for 25 objects using the spectrum synthesis calculation of the C_2 band around 5165\AA . The most metal-poor objects found will make important targets for follow-up detailed chemical composition studies

based on high-resolution spectroscopy, that are likely to provide insight into the Galactic chemical evolution.

Keywords: stars: Population II, stars: Late-type, stars: carbon, stars: atmospheric parameters, stars: low-mass, stars: metallicity

1 Introduction

Very metal-poor stars play a crucial role in unraveling the chemical evolution of the early Galaxy, as they retain the chemical signatures from the nucleosynthesis processes of preceding stellar generations. Among the metal-poor stars, stars that exhibit enhancement of carbon ($[C/Fe] > 1$, [Beers and Christlieb \(2005\)](#); $[C/Fe] > 0.7$, [Aoki et al \(2007\)](#)) are known as carbon-enhanced metal-poor (CEMP) stars, and are excellent probes to study the early galactic nucleosynthesis and chemical evolution. These stars are believed to have originated from the remnants of Population III stars and act as the fossil records of their nucleosynthetic products. Particularly, the CEMP-no stars are considered bonafide second-generation stars ([Placco et al, 2015](#); [Hansen et al, 2016b](#); [Yoon et al, 2016](#)). This group exhibits the enhancement of carbon without any enhancement of heavy elements. In contrast, other sub-classes of CEMP stars such as CEMP-s, CEMP-r, and CEMP-r/s stars exhibit enhancement of neutron-capture elements.

While CEMP-s stars show enhancement of slow-neutron capture(s-) process elements, CEMP-r stars exhibit enhancement of rapid neutron-capture(r-) process elements. CEMP-r/s sub-group shows enhancements of both s- and r-process elements. Studies on CEMP-s and CEMP-r/s stars can give insight into the formation and evolution of low- and intermediate-mass stars. Many studies have shown that these stars are found in binary systems ([McClure and Woodsworth, 1990](#); [Preston and Sneden, 2001](#); [Hansen et al, 2016b](#); [Jorissen et al, 2016a](#); [Purandardas and Goswami, 2021b](#)), and their peculiar surface chemical compositions are attributed to the mass transfer from their binary companions. Understanding of the formation and evolution of low- and intermediate- mass stars are of special significance as they can give important clues regarding the galactic chemical evolution. About half of the heavy elements in our galaxy were produced by the low- and intermediate-mass stars during their evolution and while passing through their asymptotic giant branch (AGB) phase of evolution ([Lugaro et al, 2003](#); [Herwig, 2005](#); [Karakas and Lattanzio, 2014](#)). The origin of CEMP-r stars remains unclear, potentially linked to core-collapse supernovae and neutron star mergers that are the known sources of the r-process elements([Arcones and Thielemann, 2013](#); [Rosswog et al, 2014](#); [Abbott et al, 2017](#); [Drout et al, 2017](#); [Shappee et al, 2017](#)). Thus CEMP stars play an important role as the tracers of neutron-capture nucleosynthesis. CEMP stars, especially CEMP-s stars, outnumber CEMP-r/s and CEMP-r stars. CEMP-r stars are particularly rare([Hansen et al, 2011](#)). [Beers and Christlieb \(2005\)](#) provide an extensive review on metal-poor stars and classification of CEMP stars based on the abundances of barium and europium. [Goswami](#)

et al (2021) present a recent discussion on the classification scheme of CEMP stars, distinguishing between CEMP-s and CEMP-r/s stars.

CEMP stars represent a subgroup of carbon stars, easily identified through low-resolution spectra. The spectra of carbon stars are characterized by the dominant Swan bands of C_2 molecules and other carbon compounds such as CH and CN, and these features are easily detectable on the spectra of cool carbon stars. Bidelman (1956) introduced CH stars as a distinct group of carbon stars that show a strong CH band in the spectra. CEMP-s stars are recognized as the metal-poor counterparts of CH stars (Lucatello et al, 2005; Abate et al, 2016). Furthermore, Jorissen et al (2016b) showed that CH and CEMP-s stars fall in the same region of the period–eccentricity diagram and represent similar mass-function distributions. Based on these findings, they suggest treating CH and CEMP-s stars as a unique stellar family. These groups of stars are found to exhibit enhanced neutron-capture elements, particularly s-process elements. The origin of their peculiar surface chemical composition is attributed to their binary companion. Many studies have shown that most of the CH stars are in binary systems in which the primary companion is now an invisible white dwarf that once transferred the nucleosynthesis materials to the secondary star (CH/CEMP-s stars) during its AGB phase (McClure and Woodsworth, 1990; Preston and Sneden, 2001; Hansen et al, 2016b; Jorissen et al, 2016a; Purandardas and Goswami, 2021b).

Besides CH stars, carbon stars are further classified into C-N, C-J, and C-R groups based on spectral properties. C-N stars exhibit strong depression of light in the violet region of their spectra, lower effective temperatures, and strong molecular bands compared to C-R stars (Barnbaum et al (1996), Goswami (2005), Goswami and Aoki (2010)). The carbon isotopic ratios exhibited by most of the C-N stars lie in the range 30 to 100, while CH, and C-R stars show $^{12}C/^{13}C$ in the ranges 20-100, and 4-9 respectively (Lambert et al, 1986). Classification based on isotopic ratios would however require high-resolution spectra.

Among the C-R stars and CH stars, the presence of the strong Ca I line at 4226 Å in C-R stars distinguishes them from CH stars (Goswami, 2005). High-resolution spectroscopy indicates that C-R stars exhibit heavy element abundances similar to the Sun, unlike CH stars.

Carbon stars that are characterized by strong Merrill-Sanford (M-S) bands due to SiC_2 in their spectra are known as C-J group of stars. These bands are generally absent in the spectra of CH stars, and a few C-N stars show the presence of SiC_2 band. Similar to C-R stars, C-J stars are also found to exhibit a low carbon isotopic ratio, typically below 15 (Goswami, 2005; Goswami et al, 2007, 2010). Although many high-resolution spectroscopic analyses are available for CH stars (Pereira and Junqueira, 2003; Aoki et al, 2007; Purandardas et al, 2019; Karinkuzhi and Goswami, 2014, 2015), such studies are quite scanty for C-R, and C-J stars.

Christlieb et al (2001) compiled a list of faint high-latitude carbon (FHLC) stars, potentially containing various sub-groups of carbon stars. Distinguishing between these classes is crucial for understanding their astrophysical implications. Hence, we have undertaken to identify stars belonging to the different sub-groups of carbon stars and to derive their stellar atmospheric parameters, and carbon abundances by selecting objects from this list.

In this work, we have sampled 88 carbon stars taken from [Christlieb et al \(2001\)](#), and classified 65 of them for the first time using low-resolution spectra and estimated their atmospheric parameters and carbon abundances whenever possible. The remaining 23 stars were already classified into different sub-groups of carbon stars by [Goswami \(2005\)](#) and [Goswami et al \(2007, 2010\)](#). We have derived stellar atmospheric parameters for these stars and also the carbon abundance whenever possible. In this paper, we present the results of these analyses. The paper is arranged as follows: observations and data reductions are described in Section 2. Spectral characteristics and classifications of these stars are presented in Section 3. In Section 4 we have described methods used for the determination of the stellar atmospheric parameters. Determination of carbon abundance is discussed in Section 5, and discussions and conclusions are presented in Section 6.

2 Observations and Data Reduction

The programme stars are selected from the list of stars from HES survey and particularly from the list of faint high-latitude carbon stars of [Christlieb et al \(2001\)](#). The spectra were obtained using the Himalayan Faint Object Spectrograph Camera (HFOSC) attached to 2-m Himalayan Chandra Telescope (HCT) at the Indian Astronomical Observatory (IAO), Hanle during 2010 to 2021. The stars were selected based on their observability using this facility. HFOSC is an optical imager cum spectrograph used for low- and medium- resolution grism spectroscopy. The grism and the camera combinations used for the observations provide a spectral resolution $R (\lambda/\delta\lambda) \sim 1330$ for grism 7 and ~ 2190 for grism 8. We have obtained spectra using grism 7 and 8 that cover the wavelength regions from 3800 - 6840 Å and 5800 - 8350 Å respectively. Observations of Fe-Ar and Fe-Ne hollow cathode lamps taken immediately before and after the stellar exposures are used for wavelength calibrations. The spectra of the stars used for the comparison and identification of the spectral type of the program stars were obtained during earlier observation cycles using the same observational set-up. Data reduction was performed following the standard procedures using IRAF¹ software spectroscopic reduction package. For each object, minimum of two spectra each of 30 minutes exposures were taken and combined to increase the signal-to-noise ratio.

3 Spectral classification of the programme stars

We obtained low-resolution spectra for 65 stars and categorized them into distinct groups using well defined spectral criteria outlined in [Goswami \(2005\)](#). Key features considered include the strength of the CH band around 4300 Å, prominence of secondary P-branch head near 4342 Å, strength of the Ca I feature at 4226 Å and isotopic band depths of C₂ and CN molecular bands. Objects are classified into various sub-groups by a thorough comparison of the program stars' spectra with those of well-known CH, C-R, C-N, and C-J stars obtained under the same observational setup

¹IRAF is distributed by the National Optical Astronomical Observatories, which is operated by the Association for Universities for Research in Astronomy, Inc., under contract to the National Science Foundation

Table 1 HE stars with prominent C₂ molecular bands

Star No.	RA(2000)	Dec.(2000)	<i>l</i>	<i>b</i>	B	V	J	H	K	Bands noticed	Obs. date	Class
HE 0002+0053*	00 05 24.99	01 10 03.82	99.71	-59.61	15.02	13.3	11.02	10.38	10.12	C ₂ , CH, CN	06.11.04 20.10.20 21.07.21	C-R
HE 0017+0055*	00 20 21.59	01 12 06.81	106.9	-60.69	12.99	11.66	9.31	8.68	8.49	C ₂ , CH, CN	15.11.03 21.10.20 14.09.21	CH/CEMP-r/s
HE 0228-0256**	02 31 15.6	-02 43 06.45	171.59	-55.85	16.69	14.7	12.51	11.81	11.53	C ₂ , CH, CN	18.01.09	CN
HE 0037-0654*	00 40 01.98	-06 38 12.39	114.85	-69.33	16.69	15.50	14.15	13.71	13.72	C ₂ , CH, CN	21.10.20	CH/CEMP-s
HE 0039-2635	00 41 39.7	-26 18 53	52.81	-87.67	13.10	-	10.571	10.11	9.99	C ₂ , CH, CN	06.12.16	CH/CEMP-r/s
HE 0113+0110	01 15 52.2	+01 26 21	135.54	-60.83	16.30	15.00	13.02	12.36	12.23	C ₂ , CH, CN	06.12.16	CH/CEMP-r/s
HE 0155-0221	01 57 33.7	-22 07 06	198.09	-74.17	17.00	15.30	12.73	12.07	11.92	C ₂ , CH, CN	06.12.16	CH/CEMP-r/s
HE 0206-1916***	02 09 19.63	-19 01 55.45	192.69	-70.37	15.13	13.99	12.24	11.76	11.66	C ₂ , CH, CN	23.10.05	CH/CEMP-s
HE 0237-0835	02 40 13.6	-08 22 18	181.93	-58.16	16.80	15.60	13.71	13.14	12.99	C ₂ , CH, CN	19.12.12	CH/CEMP-r/s
HE 0251-2118	02 53 42.6	-21 05 59	207.41	-61.53	14.30	13.30	11.48	10.96	10.82	C ₂ , CH, CN	06.12.16	CH/CEMP-s
HE 0258-0218	03 01 04.9	-02 06 17	179.62	-50.14	15.90	14.80	13.48	12.88	12.79	C ₂ , CH, CN	21.12.12	CH/CEMP-r/s
HE 0319-0215*	03 21 46.26	-02 04 33.95	184.58	-46.16	15.03	13.60	11.78	11.22	11.06	C ₂ , CH, CN	17.11.20	CH/CEMP-r/s
HE 0322-1504*	03 24 40.10	-14 54 24.35	201.89	-52.38	15.81	14.29	12.1	11.53	11.34	C ₂ , CH, CN	06.11.04	CH/CEMP-s
HE 0323-2702	03 26 04.6	-26 51 38	221.55	-55.69	16.60	15.10	13.61	13.07	12.97	C ₂ , CH, CN	07.12.16	CH/CEMP-r/s
HE 0326-2603	03 28 19.68	-25 53 19.01	220.02	-55.02	16.12	15.10	13.67	13.24	13.17	C ₂ , CH, CN	20.10.20 14.09.21	CH/CEMP-r/s
HE 0333-1819*	03 35 18.87	-18 09 53.30	208.37	-51.32	13.17	11.53	9.43	8.86	8.68	C ₂ , CH, CN	20.10.20 15.09.21	CH/CEMP-s
HE 0422-2518	04 24 38.42	-25 12 10.04	223.27	-42.48	-	-	10.81	10.29	10.10	C ₂ , CH, CN	16.09.03	CH /CEMP-s
HE 0429+0232*	04 31 53.74	02 39 00.49	192.72	-29.17	14.65	13.3	11.09	10.52	10.32	C ₂ , CH, CN	16.09.03	CH/CEMP-s
HE 0507-1653*	05 09 16.56	-16 50 04.69	217.54	-29.95	13.63	12.51	10.88	10.43	10.31	C ₂ , CH, CN	06.11.04 17.11.20	CH/CEMP-r/s
HE 0507-1430	05 10 07.6	-14 26 32	215.09	-28.84	13.20	14.40	12.32	11.72	11.57	C ₂ , CH, CN	20.12.12	CH/CEMP-r/s
HE 0516-2515	05 18 09.4	-25 12 25	227.49	-30.86	15.20	13.90	11.25	10.59	10.35	C ₂ , CH, CN	06.12.16	CH/CEMP-r/s
HE 0518-2322*	05 20 35.57	-23 19 14.26	225.62	-29.74	14.07	12.79	11.15	10.67	10.57	C ₂ , CH, CN	15.11.03	CH/CEMP-s
HE 1008-0946	10 11 22.4	-10 01 13	251.16	36.29	16.80	15.80	13.22	12.63	12.49	C ₂ , CH, CN	06.12.16	CH/CEMP-r/s
HE 1023-1504***	10 25 55.55	-15 19 17.08	258.78	34.79	16.26	14.40	12.32	11.61	11.42	C ₂ , CH, CN	30.03.05	CH/CEMP-s
HE 1045-1434**	10 47 44.18	-14 50 22.52	263.59	38.40	15.83	14.60	12.93	12.44	12.24	C ₂ , CH, CN	24.02.20 21.4.21	CH/CEMP-r/s
HE 1104-0957*	11 07 19.40	-10 13 15.89	265.35	44.92	12.12	10.76	8.26	7.56	7.32	C ₂ , CH, CN	24.02.20	C-R
HE 1112-2557	11 15 14.10	-26 13 27.76	277.44	31.84	14.89	13.60	11.54	11.00	10.85	C ₂ , CH, CN	17.05.16	CH/CEMP-s
HE 1150-2546	11 53 15.48	-26 03 41.43	286.94	34.99	13.17	11.93	9.89	9.35	9.23	C ₂ , CH, CN	17.05.16	CH/CEMP-s
HE 1152-2432	11 54 34.92	-24 48 44.11	286.88	36.28	12.45	10.91	9.41	8.83	8.68	C ₂ , CH, CN	30.03.17	CH/CEMP-s
HE 1152-0355***	11 55 06.05	-04 12 24.59	277.32	55.84	13.89	11.43	10.24	8.66	8.43	C ₂ , CH, CN	24.02.20	CH/CEMP-s
HE 1157-0518	12 00 18.1	-05 34 43	280.33	55.03	15.00	15.30	13.42	12.92	12.85	C ₂ , CH, CN	17.05.16	CH/CEMP-r/s
HE 1158-0708	12 00 49.2	-07 25 33	281.59	53.34	16.20	15.00	13.38	12.62	12.48	C ₂ , CH, CN	30.03.17	CH/CEMP-r/s
HE 1205-0417	12 07 51.8	-04 34 39	282.92	56.59	16.70	15.70	12.63	11.88	11.68	C ₂ , CH, CN	01.03.13	CH/CEMP-r/s
HE 1205-0849	12 08 29.0	-09 05 50	285.42	52.30	13.90	12.60	10.80	10.18	10.03	C ₂ , CH, CN	01.03.13	CH/CEMP-s
HE 1205-0521	12 07 53.08	-05 37 50.90	283.50	55.58	15.49	14.40	12.42	11.98	11.80	C ₂ , CH, CN	24.02.20	C-R
HE 1212-0323	12 15 29.1	-03 40 23	285.82	57.99	12.70	15.0	13.04	12.43	12.29	C ₂ , CH, CN	30.03.17	CH/CEMP-r/s
HE 1221-0651	12 23 50.0	-07 07 54	290.91	55.09	15.80	14.8	13.04	12.42	12.31	C ₂ , CH, CN	05.03.10	CH/CEMP-r/s
HE 1236-0337	12 39 04.6	-03 54 25	296.97	58.82	14.10	15.40	13.23	12.61	12.43	C ₂ , CH, CN	17.04.17	CH/CEMP-r/s
HE 1241-0337	12 44 27.20	-03 54 01.19	299.55	58.92	15.80	14.30	11.87	11.23	11.01	C ₂ , CH, CN	14.04.20	CH/CEMP-r/s
HE 1251-2313	12 54 31.0	-23 29 35	303.84	39.37	14.40	13.50	11.85	11.38	11.25	C ₂ , CH, CN	17.04.17	CH /CEMP-s
HE 1255-2324	12 58 01.2	-23 40 24	304.87	39.17	11.70	-	8.66	8.17	8.00	C ₂ , CH, CN	24.01.10	CH/CEMP-s
HE 1305+0007***	13 08 03.85	-00 08 47.50	311.94	62.43	13.98	12.22	10.24	9.75	9.60	C ₂ , CH, CN	29.01.05	CH/CEMP-s
HE 1308-1012	13 11 10.9	-10 28 35	310.85	52.09	14.60	13.70	12.42	11.97	11.87	C ₂ , CH, CN	17.04.17	CH/CEMP-r/s
HE 1318-1657	13 21 19.4	-17 13 40	313.06	45.05	13.30	14.40	12.51	11.99	11.81	C ₂ , CH, CN	20.12.12	CH/CEMP-r/s
HE 1319-1935	13 22 38.70	-19 51 11.61	312.89	42.41	15.69	14.19	12.33	11.76	11.68	C ₂ , CH, CN	13.05.20	CH/CEMP-r/s
HE 1336+0200	13 38 41.2	+01 45 23	328.97	62.21	17.30	14.90	11.76	10.92	10.67	C ₂ , CH, CN	18.04.16	C-R
HE 1406-2016	14 09 44.17	-20 30 56.31	326.64	38.72	15.48	14.20	12.09	11.55	11.42	C ₂ , CH, CN	17.05.16	CH/CEMP-s
HE 1429-0551*	14 32 31.29	-06 05 00.20	343.01	48.76	14.01	12.61	10.73	10.27	10.07	C ₂ , CH, CN	13.05.20 07.04.21	CH /CEMP-r/s
HE 1430+0227	14 32 46.5	+02 14 44	351.53	55.25	17.10	15.90	14.02	13.48	13.31	C ₂ , CH, CN	17.05.16	CH/CEMP-r/s
HE 1431-0245	14 33 54.2	-02 58 33	346.32	51.05	16.20	15.30	13.57	13.01	12.99	C ₂ , CH, CN	19.02.17	CH/CEMP-r/s
HE 1442-0346	14 45 02.1	-03 58 46	348.10	48.53	16.30	15.40	13.75	13.25	13.11	C ₂ , CH, CN	17.05.16	CH/CEMP-r/s
HE 1523-1155*	15 26 41.04	-12 05 42.66	351.87	35.63	14.57	13.22	11.37	10.85	10.75	C ₂ , CH, CN	13.04.20	CH/CEMP-r/s
HE 1528-0409*	15 30 54.30	-04 19 40.36	359.86	40.29	16.00	14.76	12.94	12.45	12.36	C ₂ , CH, CN	13.05.20	CH/CEMP-r/s
HE 2145-1715*	21 48 44.46	-17 01 02.46	36.63	-46.73	14.59	13.20	11.03	10.36	10.25	C ₂ , CH, CN	17.09.03	CH/CEMP-s
HE 2150-1800	21 53 17.55	-17 46 38.92	36.16	-48.01	15.76	14.78	13.24	12.79	12.70	C ₂ , CH, CN	20.10.20	CH/CEMP-s
HE 2218+0127*	22 21 26.05	01 42 19.81	65.46	-43.8	14.80	14.00	11.83	11.51	11.43	C ₂ , CH, CN	16.09.03	CH/CEMP-s
HE 2319-0852	23 22 17.32	-08 36 16.94	70.07	-61.93	-	15.20	13.46	12.99	12.82	C ₂ , CH, CN	20.10.2020	CH/CEMP-s
HE 2331-1329*	23 33 44.51	-13 12 33.74	66.55	-67.12	16.79	14.50	11.84	10.99	10.65	C ₂ , CH, CN	17.11.20 3.12.20	CN
HE 2339-0837*	23 41 59.93	-08 21 18.60	78.51	-65.05	15.32	14.00	12.63	12.11	12.03	C ₂ , CH, CN	21.10.20	CH/CEMP-r/s

* Goswami (2005), ** Goswami et al (2010), *** Goswami et al (2007)

Table 2 HE stars without prominent C₂ molecular bands

Star No.	RA(2000)	Dec.(2000)	<i>l</i>	<i>b</i>	B	V	J	H	K	Bands noticed	Obs. date
HE 0341-0314	03 44 13.5	-03 04 39	190.36	-42.25	17.0	16.4	14.245	13.667	13.450	CH,CN	23.10.15
HE 0359-0141*	04 02 21.30	-01 33 03.96	192.03	-37.64	14.66	13.3	11.07	10.44	10.25	CH,CN	15.11.03
HE 0417-0513*	04 19 46.83	-05 06 17.21	198.66	-35.82	15.01	13.7	11.17	10.52	10.38	CH,CN	15.11.03
HE 0432-0923	04 34 25.67	-09 16 50.51	205.26	-34.60	-	15.16	13.52	13.04	12.97	CH,CN	18.03.21
HE 0443-1847*	04 46 10.89	-18 41 39.63	217.23	-35.75	14.17	12.9	10.7	10.17	10.01	CH,CN	16.09.03
HE 0503-2009***	05 06 02.95	-20 05 57.35	220.77	-31.84	14.3	13.1	11.15	10.62	10.49	CH, CN	23.10.05
HE 0508-1604*	05 10 47.01	-16 00 39.39	216.82	-29.31	13.25	11.65	9.9	9.33	9.16	CH,CN	20.12.04
HE 0518-1751*	05 20 28.46	-17 48 42.67	219.71	-27.84	13.85	12.8	10.65	10.11	9.97	CH,CN	07.11.04
HE 0519-2053*	05 21 54.42	-20 50 35.31	223.06	-28.62	14.88	13.7	11.96	11.39	11.29	CH,CN	15.11.03
HE 0919+0200*	09 22 13.07	01 47 55.78	230.52	33.93	13.91	12.6	10.67	10.1	9.95	CH,CN	03.03.04
HE 0926-0417	09 29 10.3	-04 30 44	237.91	31.84	14.1	13.3	11.631	11.107	10.999	CH,CN	06.12.16
HE 0930-0018*	09 33 24.63	-00 31 44.62	234.74	35.01	16.13	14.7	12.19	11.54	11.33	CH,CN	02.03.04
HE 0930-0945	09 32 40.6	-09 58 48	243.56	29.21	14.5	13.4	11.66	11.11	11.00	CH,CN	19.02.17
HE 1032-1655	10 34 36.5	-17 10 59	262.17	34.64	13.7	-	10.854	10.256	10.134	CH,CN	19.02.17
HE 1058-1300	11 00 37.2	-13 16 55	265.79	41.46	14.1	13.2	11.231	10.659	10.497	CH,CN	19.02.17
HE 1130-1956	11 32 52.7	-20 13 25	278.99	38.97	15.0	13.6	11.604	11.079	10.946	CH,CN	17.04.17
HE 1150-2049	11 53 27.7	-21 05 50	285.24	39.77	15.7	15.0	13.103	12.542	12.422	CH,CN	06.03.16
HE 1208-1247	12 10 55.1	-13 04 09	287.91	48.62	14.4	13.5	11.588	10.949	10.811	CH,CN	30.03.17
HE 1212-1414	12 14 51.8	-14 31 15	289.79	47.42	15.9	-	9.708	9.088	8.941	CH,CN	19.02.17
HE 1238-1714	12 40 46.3	-17 31 17	299.32	45.27	15.0	-	8.924	8.391	8.253	CH,CN	17.04.17
HE 1244-3036	12 47 39.23	-30 53 16.06	301.97	31.97	14.53	13.60	12.03	11.54	11.46	CH,CN	18.03.21
HE 1247-2554	12 50 20.7	-26 10 38	302.63	36.69	13.2	-	10.153	9.554	9.377	CH,CN	17.04.17
HE 1318-2451	13 20 57.7	-25 07 30	311.33	37.26	15.4	-	10.236	9.681	9.538	CH,CN	19.02.17
HE 1319-2340	13 21 43.9	-23 56 27	311.77	38.41	15.3	13.6	11.461	10.937	10.795	CH,CN	05.10.12
HE 1345-2616	13 48 02.1	-26 31 12	318.35	34.65	12.9	-	9.855	9.276	9.099	CH,CN	30.03.17
HE 1354-2552	13 56 55.1	-26 07 35	320.80	34.46	13.2	-	10.114	9.528	9.360	CH,CN	17.04.17
HE 2138-1616*	21 41 16.61	-16 02 39.85	36.95	-44.7	14.91	13.9	11.9	11.45	11.32	CH,CN	16.09.03
HE 2224-0330*	22 26 47.82	-03 14 57.48	61.22	-48.01	14.58	13.5	11.82	11.36	11.26	CH,CN	16.09.03
HE 2352-1906*	23 54 49.02	-18 49 31.13	62.49	-74.57	13.21	12.07	10.16	9.65	9.51	CH,CN	16.09.03
											03.12.20

* Goswami (2005), *** Goswami et al (2007)

and resolution. Additionally, low-resolution spectra of carbon stars from the spectral atlas of Barnbaum et al (1996) were employed.

For comparative analysis and classification, we utilized the low-resolution spectra of established CH stars such as HD 26, HD 5223, and HD 209621, C-R stars RV Sct, HD 156074, and HD 76846, and CN stars Z Psc, and V460 Cyg. From the comparison, we have found that our sample consists of 11 stars showing spectral features similar to those of HD 26, 13 objects showing similarities to HD 5223, and 10 stars resembling HD 209621. Two objects show spectral features similar to the C-R star RV Sct. We selected these comparison stars because they have been extensively studied by various authors and classified based on high-resolution spectroscopy. For example, from a detailed high-resolution spectroscopic analysis, Goswami et al (2016) have shown that HD 26 displays the characteristic properties of CH stars with a larger enhancement of the second peak s-process elements such as Ba, La, Ce, Nd, Sm compared to the first-peak s-process elements Sr, Y and Zr. Compared to the Sun ($[\text{Sr}/\text{Ba}] = 0.74$), this object shows a much smaller ratio of $[\text{Sr}/\text{Ba}] \sim -0.04$. With estimated $[\text{Ba}/\text{Eu}] \sim 1.32$ and metallicity $[\text{Fe}/\text{H}] \sim -1.13$ (Goswami et al, 2016) this object can be placed in the CEMP-s sub-group following the classification criteria of Beers and Christlieb (2005). It is to be noted that stars with $[\text{C}/\text{Fe}] > 1.0$ and $[\text{Fe}/\text{H}] < -1.0$ are termed as CEMP stars by Beers and Christlieb (2005). High resolution spectroscopic analysis by Goswami et al (2006) have shown that the object HD 5223 also exhibits the characteristic properties of CH stars. However, with an estimated metallicity $[\text{Fe}/\text{H}] \sim -2.05$

and following the classification criteria of [Beers and Christlieb \(2005\)](#) the object can be placed among the CEMP-s sub-group. A detailed high resolution spectroscopic study by [Goswami and Aoki \(2010\)](#) have shown that, although, HD 209621 shows characteristics of CH stars in terms of enhancement of heavy s-process elements relative to the lighter s-process elements, the estimated $[\text{Ba}/\text{Eu}]=+0.35$ places the star in the group of CEMP-r/s stars. High-resolution spectroscopic analysis of RV Sct by [Zamora et al \(2009\)](#) showed that this object is a late-R type star with solar metallicity.

Out of the 65 objects we have analysed, the spectra of 29 objects are found to exhibit no prominent C_2 molecular bands, rendering them unclassifiable based on the adopted spectral criteria. Among the rest which were previously classified into different sub-groups of carbon stars by [Goswami \(2005\)](#) and [Goswami et al \(2007, 2010\)](#), the objects HE 0017+0055, HE 0206–1916, HE 0228–0256, HE 0037-0654, HE 0319-0215, HE 0322–1504, HE 0333-1819, HE 0429+0232, HE 0507–1653, HE 1023–1504, HE 1045-1434, HE 1104–0957, HE 1152–0355, HE 1305+0007, HE 1429–0551, HE 1523–1155, HE 1528-0409, HE 2145–1715, HE 0518–2322, HE 2218+0127, HE 2331–1329, and HE 2339–0837 were classified as potential CH star candidates. While two objects HE 0002+0053 and HE 1104-0957 were classified as C-R stars, HE 0228–0256 and HE 2331-1329 were classified as CN stars. These authors could not classify the objects into CEMP sub-groups due to the unavailability of metallicity estimates for their sample as well as the lack of high-resolution abundance results for comparison. In this study, we have reevaluated their classification, and assigned the objects to distinct CEMP sub-groups. We have used the criteria $[\text{Fe}/\text{H}] \leq -1$ of [Beers and Christlieb \(2005\)](#) for classifying the potential CH star candidates into different CEMP sub-groups using our metallicity estimates as discussed in detail in Section 4. Furthermore, we confirmed the CEMP sub-groups of the program stars by comparing their spectra with those of the comparison stars, as discussed in the subsequent sub-sections. Thus, this classification relies solely on visual comparisons between the spectra of the program stars and the spectra of the comparison stars, as well as the metallicity estimates. Additional high-resolution measurements of various elemental abundance ratios would be useful to confirm their classification.

The basic data of the programme stars with prominent C_2 molecular bands in their spectra and their class are listed in Table 1 and those without are presented in Table 2. Classification and the description of the spectra of the objects listed in Table 1 are presented in the following sub-sections.

3.1 Candidate CH, CEMP-s and CEMP-r/s stars : Description of the spectra

HE 1406-2016, HE 1150–2546, HE 1112–2557, HE 0422–2518, HE 1205–0849, HE 1152–2432, HE 1251–2313, HE 1255–2324, and HE 0251–2118, HE 2150–1800, HE 2319–0852

The spectra of these stars closely resemble the spectrum of the star HD 26. The strength of Ca I line at 4226 Å is found to be similar in all these stars. The CH bands around 4300 Å are found to be of similar strength in all these objects and closely match with that of HD 26. The other carbon molecular bands such as CN band around 4215 Å, and C_2 bands around 4730, 5165, and 5635 Å in these stars are also of similar

strength to that of HD 26 except for a few objects. While the objects HE 0251–2118, HE 1251–2313, HE 1255–2324, and HE 2218–0127 exhibit relatively stronger C₂ band around 4730 Å, the object HE 1406–2016 shows stronger C₂ band around 5165 Å. The recent high-resolution studies by [Roriz et al \(2023\)](#) also confirms the star HE 1255-2324 as a CH star.

HE 1406–2016, HE 1150–2546, HE 1112–2557, HE 1205–0849, HE 1255–2324, and HE 2319–0852 show relatively stronger Na D line at 5890 Å in their spectra than that in HD 26. In HE 1251–2313, and HE 0251–2118, the Na D line is found to be weaker than that in HD 26. The strengths of H- α and H- β lines are of similar strengths in these stars, except for HE 0251–2118, HE 1406–2016, HE 1150–2546, HE 1205–0849, and HE 1255–2324 where these lines are found to be weaker. Ba II at 6496 Å is found to be very strong in HE 1112–2557, HE 1205–0849, and HE 1255–2324. Examples of the spectra of the program stars that resemble closely the spectrum of the CH star HD 26 are shown in Figure 1.

HE 0155–0221, HE 0258–0218, HE 0237–0835, HE 0323–2702, HE 1442–0346, HE 1318–1657, HE 1431–0245, HE 1221–0651, HE 1308–1012, HE 1212–0323, HE 1430+0227, HE 1157–0518, and HE 0507–1430.

The spectra of these stars show close match with the spectrum of HD 5223. All these stars show carbon molecular bands of similar strengths in their spectra except for HE 0237–0835, and HE 1212–0323 whose spectra show weak C₂ band around 5635 Å. The spectra of the objects HE 0237–0835, HE 0258–0218, HE 1212–0323, and HE 1318–1657 show relatively strong Ca I line at 4226 Å than that in HD 5223.

While the stars HE 0155–0221, HE 0237–0835, and HE 1430+0227 show very strong Ba II lines at 4554 Å, and 6496 Å in their spectra, HE 1308–1012 and HE 1442–0346 show relatively weaker Ba II lines. The spectra of the star HE 1442–0346 shows very weak H- α and H- β lines. Examples of the spectra of a few of these stars that resemble closely the spectrum of the star HD 5223 are shown in Figure 2.

HE 0326-2603, HE 1158–0708, HE 1008–0946, HE 0516–2515, HE 0113+0110, HE 0039–2635, HE 1205–0417, HE 1236–0337, HE 1241-0337, and HE 1319-1935

The spectra of these stars show close resemblances with the spectrum of the star HD 209621. HE 0113+0110 shows a very strong Ca I line at 4226 Å than that in HD 209621. The carbon molecular bands in these stars show similar strengths except HE 0039–2635, HE 0113+0110, HE 0516–2515, HE 1158–0708, and HE 1205–0417 where the C₂ band around 5635 Å is found to be relatively weaker.

Ba II at 4554 Å is found to be marginally weaker in HE 0039–2635, HE 0516–2515, HE 1008–0946, and HE 1158–0708 than in HD 209621. But this line along with Ba II at 6496 Å are very strong in HE 0113+0110. The spectra of HE 1158–0708, HE 1205–0417, and HE 1236–0337 show relatively weak H- α and H- β lines. While Na D lines in the spectra of HE 1205–0417 are found to be strong, the spectra of HE

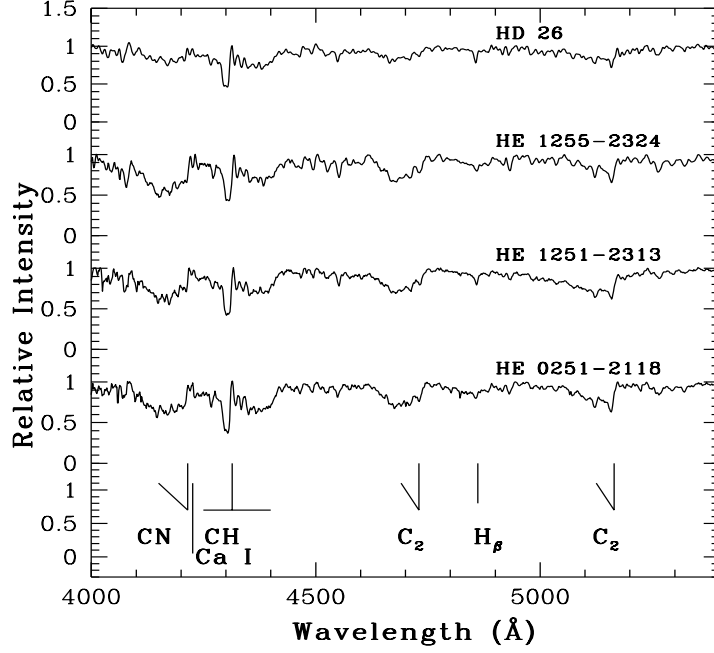


Fig. 1 Examples of the spectra of potential CH star candidates, in the wavelength region 4000 to 5400 Å that resemble closely the spectrum of the CH star HD 26

0039–2635 shows a very weak Na D line. Examples of the spectra of the program stars that resemble closely the spectrum of the star HD 209621 are shown in Figure 3.

3.2 Candidate C-R stars : Description of the spectra

HE 1205-0521, and HE 1336+0200

The spectra of these objects resemble the spectrum of the C-R star RV Sct (Figure 4). Both of them show carbon molecular bands of similar strengths. HE 1205-0521 shows relatively weak Ca I line at 4226 Å. While the spectrum of HE 1336+0200 shows relatively stronger Ba II line at 4554 Å and 6496 Å than that in RV Sct star, these lines are marginally detectable in the spectrum of HE 1205-0521. Na D line is also found to be very weak in the spectrum of HE 1205-0521. HE 1336+0200 shows relatively strong H- β line in the spectra.

4 Determination of Atmospheric parameters

Estimates of stellar atmospheric parameters the effective temperature (T_{eff}), surface gravity ($\log g$), microturbulence (ξ) and metallicity ($[Fe/H]$) are crucial for the comprehensive characterization and classification of stars. These parameters play a pivotal role in unraveling the nucleosynthesis processes and understanding the various evolutionary stages. We could derive stellar atmospheric parameters for 36 stars in our sample following the methods as described in the following sub-sections. However,

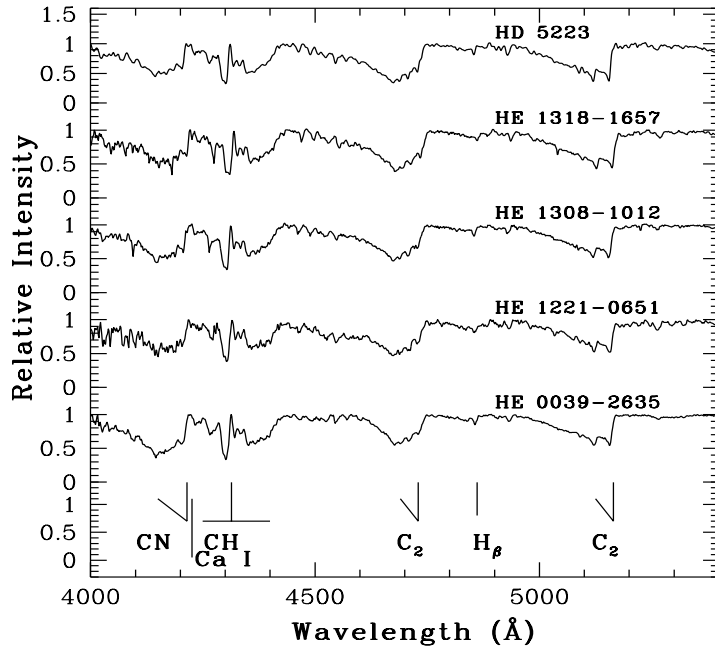


Fig. 2 Examples of the spectra of potential CH star candidates, in the wavelength region 4000 to 5400 Å that resemble closely the spectrum of HD 5223.

for the remaining stars, such determinations were challenging due to various factors. For instance, some stars fell outside the available evolutionary tracks, precluding the derivation of their mass—a key factor for determining both surface gravity and micro-turbulent velocity. Additionally, in certain cases, the H- α line was too strong and saturated, and it posed challenges in obtaining a reliable temperature value. Other instances involved the unavailability of grism 8 spectra, preventing the derivation of metallicity from the Ca II triplet (CaT) lines.

4.1 Effective temperature

Among the methods, the ones that are commonly used to derive effective temperatures are, using photometric colours, flux calibrated low-resolution spectra, and in high-resolution spectra using fitting shape of the balmer lines, and through excitation balance, i.e., forcing no trend of Fe I abundances with the excitation potential of the lines.

We have determined preliminary estimates of the effective temperatures of the programme stars using the calibration equations of [Alonso et al \(1999\)](#). These estimates are further verified through spectral synthesis of the H- α line at 6562.8 Å, whenever it was possible, using the model atmospheres selected from the Kurucz grid of model atmospheres with no convective overshooting (<http://kurucz.harvard.edu/grids.html>). Solar abundances are taken from [Asplund et al \(2009\)](#). Some examples of spectrum synthesis fits of H- α line are shown in [Figures 5](#). The photometric estimates for the

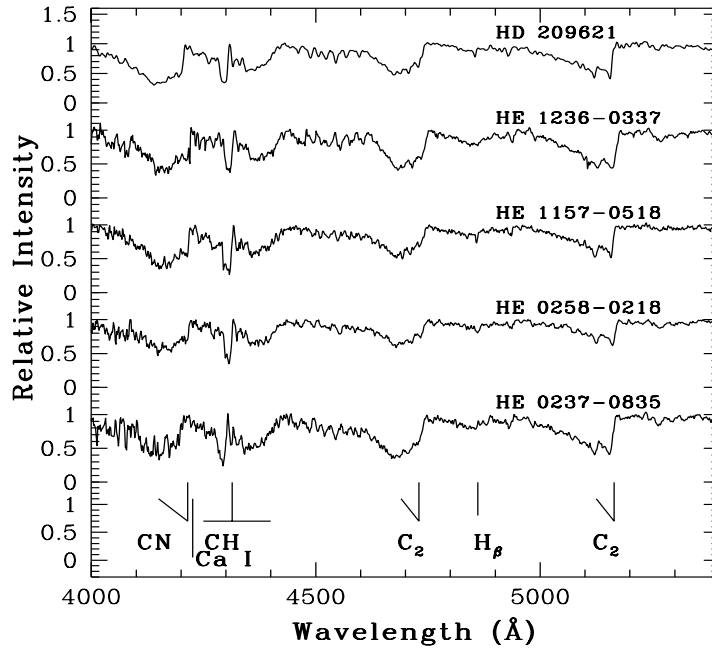


Fig. 3 Examples of the spectra of potential CH star candidates, in the wavelength region 4000 to 5400 Å that resemble closely the spectrum of HD 209621.

programme stars and their comparison with the temperature derived from the H- α line are presented in Table A1.

4.2 Surface gravity

The surface gravity $\log g$ is calculated from the mass of the star using the relation

$$\log (g/g_{\odot}) = \log (M/M_{\odot}) + 4\log (T_{eff}/T_{eff\odot}) + 0.4(M_{bol} - M_{bol\odot}).$$

The adopted values for the Sun are $\log g_{\odot} = 4.44$, $T_{eff\odot} = 5770$ K, and $M_{bol\odot} = 4.75$ mag (Yang et al, 2016). Masses of the stars are determined from their positions in the H-R diagram. For this estimation, we made use of the Girardi et al (2000) database (<http://pleiadi.pd.astro.it/>) of evolutionary tracks corresponding to the metallicity of the star. The metallicity of the star is taken to be those estimated from the CaT calibration. Parallaxes are taken from Gaia DR3 (Gaia Collaboration et al (2016, 2018) <https://gea.esac.esa.int/archive/>). The estimated masses of our program stars range from $0.83 M_{\odot}$ to $2.2 M_{\odot}$.

4.3 Microturbulence

The HERES collaboration (Barklem et al, 2005) could measure the microturbulent velocity ξ , for 254 metal-poor stars based on the analysis of high-resolution spectra.

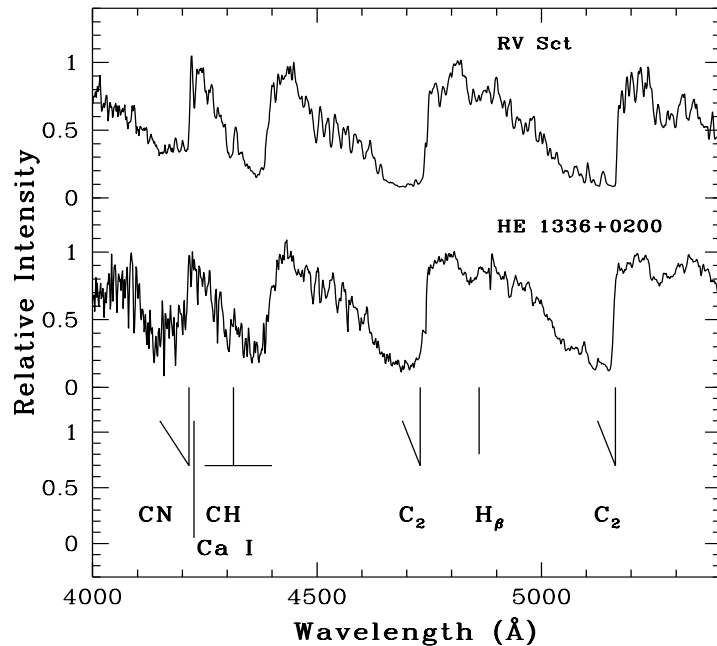


Fig. 4 The spectra of HE 1336+0200, in the wavelength region 4000 to 5400 Å that resemble closely the spectrum of the C-R star RV Sct.

Johnson et al (2007) fitted the $\log g$ and ξ values obtained by Barklem et al (2005) with a second order polynomial,

$$\xi = 2.822 - 0.669 \log g + 0.080 (\log g)^2 \text{ km s}^{-1}.$$

We made use of this relation for the estimation of the microturbulent velocity. This equation is valid for the surface gravity in the range $1 < \log g < 4.2$. The HERES data show an rms scatter of 0.17 km s^{-1} around this relation. Johnson et al (2007) found that the uncertainties in ξ do not contribute significantly to the final abundance errors.

4.4 Metallicity

The metallicities of the programme stars are determined from the CaT lines using the calibration equation provided by Carrera et al (2013). They have presented a calibration of the CaT lines as a metallicity indicator in the metallicity range $-4.0 \leq [\text{Fe}/\text{H}] \leq +0.5$, based on a tight correlation observed between $[\text{Fe}/\text{H}]$ values derived from the CaT and $[\text{Fe}/\text{H}]$ measured from high-resolution spectra as follows:

$$[\text{Fe}/\text{H}] = a + b \times \text{Mag} + c \times \sum \text{Ca} + d \times \sum \text{Ca}^{-1.5} + e \times \sum \text{Ca} \times \text{Mag},$$

where Mag represents the luminosity indicator. The values of the terms, a,b,c,d, and

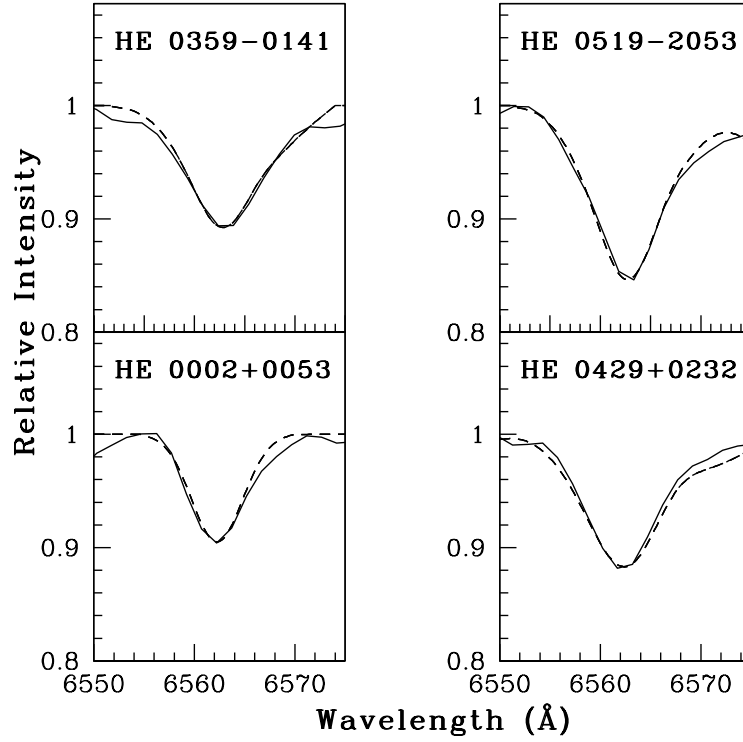


Fig. 5 Examples of spectrum synthesis fits of H_{α} line profile at 6562.8 Å. Short dashed lines represent synthesized spectra and the solid lines indicate the observed spectra.

e for each luminosity indicators are available in [Carrera et al \(2013\)](#). $\sum Ca$ is the CaT index which represents the sum of the equivalent widths of the CaT features.

We have used this relation to derive the metallicity of our program stars whenever the grism 8 spectra are available for them. These values are presented in Table 3. We have used absolute magnitude in V (M_v) as the luminosity indicator. Examples of the sample spectra of the programme stars showing the CaT lines in the wavelength region 8450 to 8700 Å are shown in Figure 6. We have also determined the CaT metallicity for different combinations of equivalent widths of CaT features for 43 stars using high-resolution spectra ($R \sim 30000, 42000$ and 60000) for which high-resolution metallicity estimates are available (Table B2). We have plotted the metallicity of 43 stars, determined through high-resolution spectroscopy (values compiled from various sources in literature, as indicated below Table B2), in relation to the variance between their metallicities calculated from the CaT lines and the corresponding high-resolution estimates (Figure 7). From this figure, we found that the metallicities corresponding to W8498+W8542+W8662 and W8542+W8662 show good agreement with the literature values.

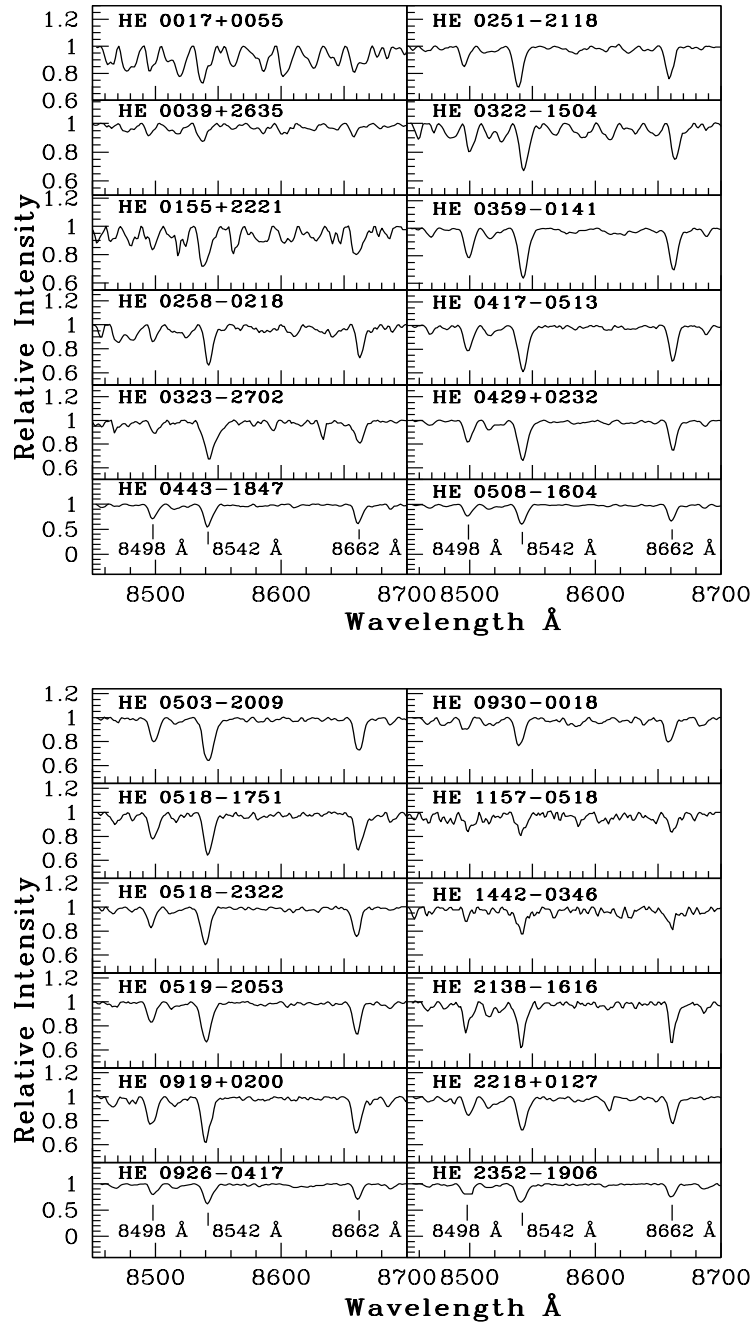


Fig. 6 Examples of the sample spectra of programme stars showing the CaT lines in the wavelength region 8450 to 8700 Å.

Table 3 Metallicity estimates from CaT lines for the programme stars

Star name	V	Parallax (mas)	Mv	W8498 (mÅ)	W8542 (mÅ)	W8662 (mÅ)	[Fe/H] (W8498+W8542+W8662) (CT1)	[Fe/H] (W8498+W8542) (CT2)	[Fe/H] (W8542+W8662) (CT3)	[Fe/H] (W8498+W8662) (CT4)	Lit.value	Reference
HE 0002+0053	13.3	0.07±0.04	-2.55±1.41	1.45	2.65	1.77	-1.77±0.38	-2.44±0.33	-2.32±0.34	-2.78±0.31	-2.18	1
HE 0017+0055	11.7	0.25±0.05	-1.31±0.39	1.5	4.63	1.27	-0.83±0.11	-1.33±0.11	-1.42±0.10	-2.7±0.08	-2.4	2
HE 0037-0654	15.5	0.15±0.03	1.47±0.50	1.73	2.02	1.22	-1.08±0.13	-1.65±0.12	-1.88±0.11	-2.03±0.11	-	-
HE 0039-2635	12.2	0.19±0.05	-1.28±2.78	0.66	1.25	0.92	-2.67±1.49	-3.11±1.18	-2.98±1.54	-3.31±1.34	-3.60	3
HE 0155-2221	15.3	0.04±0.03	-1.84±1.55	1.49	3.15	2.48	-1.1±0.74	-2.06±1.19	-1.67±1.00	-2.32±1.31	-2.28	1
HE 0206-1916	13.9	0.14±0.02	-0.28±0.28	0.52	1.36	0.94	-2.46±0.06	-2.94±0.05	-2.71±0.05	-3.20±0.05	-2.52	4
HE 0228-0256	14.7	0.008±0.04	-5.68±4.77	1.68	3.3	2.47	-2.13±1.64	-2.9±1.94	-2.65±1.84	-3.16±2.04	-	-
HE 0251-2118	13.3	0.20±0.02	-0.19±0.25	1.09	2.71	1.97	-1.17±0.07	-2.0±0.06	-1.63±0.06	-2.33±0.05	-1.50	1
HE 0258-0218	14.8	0.08±0.06	-0.56±0.67	0.82	2.75	1.48	-1.57±0.43	-2.19±0.38	-1.91±0.40	-2.77±0.34	-	-
HE 0319-0215	13.6	0.08±0.01	-1.77±0.64	0.55	1.41	0.74	-2.83±0.09	-3.19±0.08	-3.09±0.08	-3.61±0.07	-2.42	1
HE 0322-1504	14.3	1.26±0.28	4.8±0.47	1.48	3.04	2.07	-0.60±0.14	-0.47±0.12	-0.15±0.12	-0.97±0.12	-2.00	4
HE 0323-2702	15.1	0.04±0.03	-1.89±0.75	0.94	3.54	1.82	-1.44±0.94	-2.14±1.26	-1.8±1.10	-2.84±1.58	-	-
HE 0326-2603	15.1	0.20±0.02	1.66±0.38	0.43	0.76	0.26	-2.85±0.04	-3.06±0.04	-3.25±0.04	-3.82±0.04	-	-
HE 0333-1819	11.5	0.88±0.01	1.26±0.03	1.46	3.43	2.78	0.06±0.01	-1.17±0.01	-0.58±0.01	-1.46±0.01	-	-
HE 0359-0141	13.4	0.43±0.02	1.56±0.12	1.78	3.24	2.52	0.09±0.03	-1.04±0.03	-0.70±0.03	-1.32±0.03	-	-
HE 0417-0513	13.7	0.43±0.04	1.87±0.20	1.78	3.56	2.27	-0.21±0.06	-0.81±0.05	-0.59±0.06	-1.41±0.05	-1.88	1
HE 0429+0232	13.3	0.97±0.05	3.23±0.3	1.44	3.09	1.82	0.02±0.67	-0.85±0.57	-0.67±0.64	-1.48±0.57	-2.05	1
HE 0443-1847	12.9	0.45±0.03	1.19±0.06	2.25	3.73	2.90	-0.55±0.02	-0.71±0.02	-0.43±0.02	-1.08±0.01	-	-
HE 0503-2009	13.1	0.28±0.03	0.33±0.18	1.73	3.95	2.42	-0.05±0.07	-1.09±0.05	-0.78±0.06	-1.73±0.05	-	-
HE 0507-1653	12.5	0.52±0.03	1.08±0.12	0.05	2.32	1.61	-1.63±0.03	-2.4±0.03	-1.65±0.03	-2.81±0.02	-1.43	5
HE 0507-1430	14.4	0.05±0.02	-2.06±0.92	1.08	3.55	1.22	-1.66±0.25	-2.13±0.23	-2.01±0.27	-3.09±0.22	-2.4	4
HE 0508-1604	11.6	0.62±0.03	0.62±0.12	1.09	3.25	2.55	-0.47±0.03	-1.57±0.03	-0.94±0.03	-1.89±0.02	-	-
HE 0518-1751	12.8	1.16±0.03	3.12±0.06	1.20	2.79	1.87	-0.24±0.01	-1.14±0.01	-0.81±0.01	-1.61±0.01	-1.9	1
HE 0518-2322	12.8	0.25±0.02	-0.21±0.22	1.28	2.92	1.95	-1.02±0.06	-1.84±0.05	-1.55±0.05	-2.26±0.04	-	-
HE 0519-2053	13.7	0.19±0.02	0.15±0.16	0.72	1.06	3.35	-1.35±0.04	-2.91±0.03	-1.66±0.04	-1.81±0.04	-1.45	1
HE 0919+0200	12.6	0.51±0.04	1.13±0.17	2.18	3.53	2.67	-0.33±0.05	-0.83±0.05	-0.64±0.05	-1.22±0.04	-	-
HE 0926-0417	13.3	0.58±0.03	2.13±0.09	1.74	3.32	2.01	0.04±0.03	-0.88±0.02	-0.75±0.03	-1.49±0.02	-	-
HE 0930-0018	14.7	5.68±0.03	8.47±0.01	0.91	2.08	1.83	-0.61±0.005	-0.49±0.005	0.009±0.005	-0.68±0.01	-	-
HE 1045-1434	14.6	0.07±0.02	-1.02±0.60	0.91	1.19	0.82	-2.58±0.12	-2.97±0.12	-3.01±0.11	-3.17± 0.11	-2.50	4
HE 1104-0957	10.8	0.26±0.02	-2.17±0.17	1.14	2.11	1.09	-2.25±0.04	-2.69±0.04	-2.71±0.03	-3.13±0.03	-	-
HE 1152-0355	11.4	0.13±0.02	-2.99±0.38	0.89	2.37	1.38	-2.34±0.09	-2.87±0.08	-2.67±0.09	-3.28±0.08	-1.27	6
HE 1157-0518	15.1	0.08±0.04	-0.42±0.22	1.62	1.80	1.55	-1.56±0.30	-2.23±0.27	-2.26±0.27	-2.34±0.27	-2.39	5
HE 1205-0521	14.4	0.03±0.02	-3.14±0.30	0.90	2.07	1.27	-2.52±0.52	-3.01±0.47	-2.87±0.48	-3.36±0.43	-	-
HE 1205-0849	12.6	0.35±0.01	0.34±0.09	1.44	3.24	2.27	-0.52±0.03	-1.49±0.02	-1.14±0.02	-1.91±0.02	-	-
HE 1319-1935	14.2	0.03±0.02	-3.68±0.90	1.03	2.48	1.73	-2.29±0.63	-2.91±0.54	-2.67±0.58	-3.22±0.51	-2.22	7
HE 1429-0551	12.6	0.21±0.01	-0.75±0.15	0.52	1.49	0.64	-2.64±0.03	-2.96±0.03	-2.89±0.03	-3.53±0.03	-2.45	8
HE 1442-0346	15.4	0.07±0.06	-0.35±2.78	0.64	1.88	1.78	-1.83±0.03	-2.62±0.57	-2.1±0.64	-2.67±0.57	-	-
HE 1523-1155	13.2	0.22±0.01	-0.05±0.13	1.63	1.58	1.04	-1.78±0.03	-2.24±0.02	-2.51±0.03	-2.48±0.02	-2.42	8
HE 1528-0409	14.8	0.18±0.03	0.99±0.32	0.19	1.41	0.66	-2.48±0.06	-2.86±0.06	-2.58±0.06	-3.61±0.06	-2.35	8
HE 2138-1616	13.9	0.69±0.04	3.11±0.14	1.69	2.51	2.07	-0.05±0.03	-1.05±0.03	-0.86±0.03	-1.26±0.03	-0.5	9
HE 2145-1715	13.2	0.03±0.05	-4.28±3.14	0.59	2.46	1.86	-2.56±1.53	-3.23±1.83	-2.77±1.62	-3.46±1.93	-1.5	1
HE 2150-1800	14.8	0.17±0.02	0.89±0.05	0.34	1.49	0.90	-2.25±0.06	-2.73±0.05	-2.42±0.05	-3.15±0.05	-	-
HE 2218+0127	14.0	1.49±0.03	4.86±0.06	1.32	2.44	1.66	0.01±0.03	-0.85±0.02	-0.67±0.02	-1.28±0.02	-	-
HE 2224-0330	13.5	0.50±0.03	2.0±0.13	1.24	3.09	2.25	-0.21±0.03	-1.24±0.03	-0.77±0.03	-1.64±0.03	-1.2	1
HE 2319-0852	15.2	0.06±0.03	-0.63±0.22	0.32	0.60	0.57	-3.24±0.22	-3.77±0.21	-3.49±0.22	-3.81±0.21	-	-
HE 2331-1329	14.5	0.22±0.02	-3.78±0.51	1.52	3.58	1.51	-1.85±0.43	-2.37±0.38	-2.38±0.39	-3.13±0.33	-	-
HE 2339-0837	14.0	0.11±0.02	-0.82±0.30	0.59	1.17	0.76	-2.71±0.08	-3.10±0.07	-3.01±0.07	-3.38±0.07	-2.71	1
HE 2352-1906	12.1	1.28±0.03	2.6±0.05	2.15	3.58	1.99	-0.49±0.01	-0.43±0.02	-0.51±0.01	-1.19±0.01	-	-

1. Kennedy et al (2011), 2. Jorissen et al (2016b), 3. Barbuy et al (1997), 4. Abate et al (2015), 5. Aoki et al (2007), 6. Goswami et al (2006), 7. Yong et al (2013), 8. Purandardas and Goswami (2021a), 9. Hansen et al (2016a)

5 Determination of carbon abundance

We determined the carbon abundance in potential CH star candidates within our sample through spectrum synthesis calculations of the carbon band at 5165 Å (Figure 8). We have made use of MOOG (Snedden (1973), updated version 2019) for the analysis under the assumption of local thermodynamic equilibrium. In most cases, CH band around 4300Å, and C₂ band around 5635 Å are found to be saturated, and hence we used the carbon band at 5165 Å whenever possible. We estimated the abundances of elements such as Mg, Ca, Ti and Ni, which have the maximum contributions in the spectral region of our interest, and are taken from Figure 7 of Goswami and Prantzos (2000). The metallicity used for the estimation of carbon abundance is listed in Table 4. We have used the metallicities corresponding to either W8498+W8542+W8662 or W8542+W8662 based on the availability of clean and symmetric CaT lines. We have also used the metallicity derived from the combination W8498+W8542 in cases where

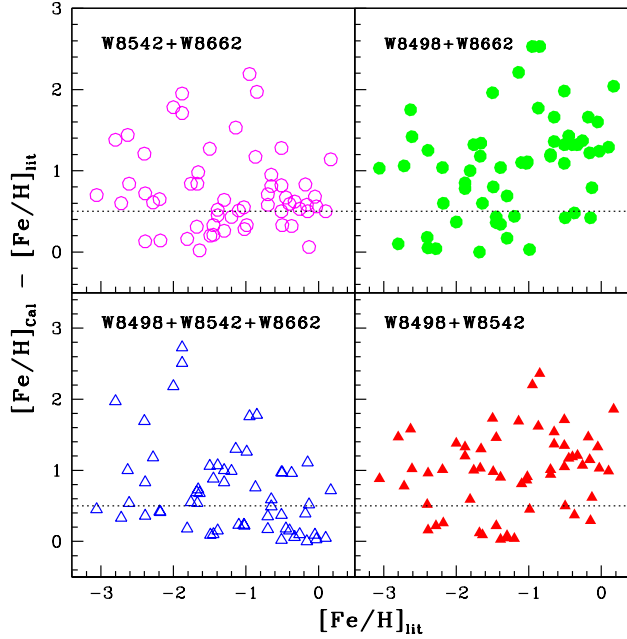


Fig. 7 Plot of metallicity, $[\text{Fe}/\text{H}]$ of stars determined from the high-resolution spectroscopic analysis (compiled from various literature, Table B2) vs. difference between their metallicities calculated from the CaT lines and that from high-resolution spectroscopic analysis. The combination of CaT lines used for the calculation of the metallicity is displayed in the corresponding panels. The short dashed line corresponds to the aforementioned difference equal to 0.5dex

the line at 8662 Å is either blended or asymmetric. The derived carbon abundances are listed in Table 5. In many cases, it was not possible to derive the carbon abundance due to various reasons, such as the carbon bands being too strong and saturated, and/or unavailability of reliable stellar atmospheric parameters for objects, as discussed in Section 4.

In light of the diagram presented in Yoon et al (2016)(their figure 1), our program stars for which carbon abundances were derived fall in the region labeled as "Group 1", just where CEMP-s and CEMP-r/s stars are found. Also, since such stars show $[\text{C}/\text{Fe}] > 1.0$ dex, they lie in the region of CEMP stars in the plot of $[\text{C}/\text{Fe}]$ vs. $\log(L/L_{sun})$ of Aoki et al (2007)(their figure 4).

6 Discussions and Conclusions

Low-resolution HCT/HFOSC spectra of a sample of 88 carbon stars are analyzed. The sample is found to contain 53 CH stars, four C-R stars, and two C-N type stars based on a set of well defined carbon star classification criteria. Twenty-nine objects in our sample do not show prominent C_2 molecular bands on their spectra. So we could not classify these stars. We could derive stellar atmospheric parameters for 36 stars in our sample. We could not derive these parameters for the remaining stars due to several

Table 4 Derived atmospheric parameters of the programme stars.

Star	T_{eff} (J-K) (K)	T_{eff} (H_{α}) (K)	log g (Parallax) (cgs)	ζ (log g-Parallax) (km s ⁻¹)	[Fe/H] (CaT)
HE 0002+0053	4070.0	4250	1.28	1.28	-1.77±0.38 (CT1)
HE 0017+0055	4261.4	4500	0.94	2.26	-1.42±0.10 (CT3)
HE 0037-0654	5458.0	-	3.07	1.52	-1.88±0.11(CT3)
HE 0039-2635	4911.7	5100	1.68	1.92	-2.67±1.49 (CT1)
HE 0155-2221	4266.0	4500	2.00	1.82	-1.67±1.0 (CT3)
HE 0206-1916	4895.0	4650	1.84	1.86	-2.71±0.05 (CT3)
HE 0228-0256	3926.2	4200	1.50	1.99	-2.65±1.84(CT3)
HE 0251-2118	4655.0	4400	1.71	1.91	-1.63±0.06 (CT3)
HE 0258-0218	4586.9	4800	1.39	2.04	-1.91±0.40 (CT3)
HE 0319-0215	-	4700	1.30	2.08	-3.09±0.08(CT3)
HE 0322-1504	4370.3	4600	1.20	2.13	-0.15±0.12 (CT3)
HE 0323-2702	4701.8	4500	1.32	2.08	-1.80±1.10 (CT3)
HE 0359-0141	4243.2	4450	2.09	1.77	-1.04±0.03 (CT2)
HE 0443-1847	4559.4	4300	2.34	1.69	-0.43±0.02 (CT3)
HE 0503-2009	4678.3	4450	2.31	1.7	-1.09±0.05 (CT2)
HE 0507-1430	4407.5	4600	0.78	2.35	-2.01±0.27 (CT3)
HE 0507-1653	4935.0	5200	2.27	1.72	-1.63±0.03 (CT1)
HE 0508-1604	4432.7	4650	2.05	1.77	-0.94±0.03 (CT3)
HE 0518-1751	4589.8	4350	2.95	1.54	-1.14±0.01 (CT2)
HE 0518-2322	4885.4	5100	1.99	1.81	-1.02±0.06 (CT1)
HE 0519-2053	4623.5	4400	2.00	1.82	-1.35±0.04 (CT1)
HE 0926-0417	4731.7	4500	2.78	1.58	-0.88±0.02 (CT2)
HE 1045-1434	4564.8	4800	1.61	1.95	-3.01±0.11 (CT3)
HE 1157-0518	4921.7	4700	1.88	1.85	-1.56±0.30 (CT1)
HE 1205-0521	4768.0	5000	1.50	1.99	-2.87±0.48(CT3)
HE 1319-1935	4678.0	-	1.01	2.23	-2.67±0.58 (CT3)
HE 1429-0551	4609.4	4800	1.61	1.96	-2.89±0.03 (CT3)
HE 1442-0346	4719.7	4950	1.62	1.95	-1.83±0.67 (CT1)
HE 1523-1155	4768.2	5000	1.81	1.87	-2.51±0.03(CT3)
HE 2138-1616	4861.9	4600	3.48	1.46	-0.86±0.03 (CT3)
HE 2145-1715	4341.2	4100	0.43	2.55	-2.56±1.53 (CT1)
HE 2150-1800	5017.1	4900	1.20	2.13	-2.25±0.06 (CT1)
HE 2218+0127	5623.3	5400	4.35	1.43	-0.67±0.02 (CT3)
HE 2224-0330	4968.8	4750	2.70	1.57	-0.77±0.03 (CT3)
HE 2339-0837	4830.7	4600	1.66	1.93	-3.01±0.07(CT3)
HE 2352-1906	4672.4	4450	2.91	1.55	-0.51±0.01 (CT3)

reasons, as discussed in Section 4. Effective temperatures were determined using both the photometric calibration equations of [Alonso et al \(1999\)](#) and the spectral synthesis of the H_{α} line at 6562 Å. Discrepancies up to 250 K for J-K temperatures and 480 K for J-H and V-K temperatures were observed between the two methods.

Several studies in the past have investigated the dependence of the strength of near-infrared CaT lines at λ 8498, 8542, and 8662 Å on stellar parameters like luminosity and metallicity ([Carrera et al \(2007, 2013\)](#) and references therein). These lines formed due to transitions between the upper $4p^2P_{1/2,3/2}$ levels and the lower meta-stable $3d^2D_{3/2,5/2}$ levels are the most conspicuous features in the near-infrared region of the spectrum and hence easy to observe even in faint stars. These lines are relatively free from blends unlike Na I lines at λ 8183.25, 8194.82 Å that are contaminated due to the presence of telluric lines. The metallicity of the 49 program stars is determined from the CaT lines using the calibration equation provided by [Carrera et al \(2007\)](#). The derived metallicities range from $-0.43 \leq [Fe/H] \leq -3.49$. Our sample consists of 19 metal-poor ($[Fe/H] \leq -1$), 14 very metal-poor ($[Fe/H] \leq -2$), and five extremely metal-poor ($[Fe/H] \leq -3$) stars. Eleven objects are found to have metallicity in the range: $-0.43 \leq [Fe/H] \leq -0.97$.

CaT metallicities were determined for 43 stars for which high-resolution spectroscopic analysis results are available. Comparisons with high-resolution estimates revealed good agreement for W8498+W8542+W8662 and W8542+W8662, with

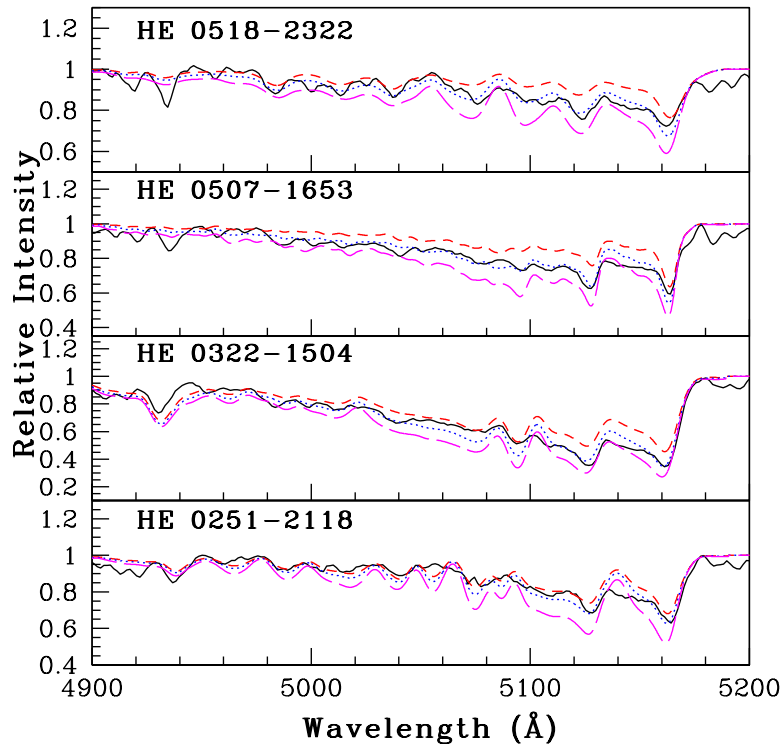


Fig. 8 Synthesis of C_2 band around 5165 Å. Dotted line represents synthesized spectra and the solid line indicates the observed spectra. Short dashed line represents the synthetic spectra corresponding to $\Delta [C/Fe] = -0.3$ and long dashed line corresponds to $\Delta [C/Fe] = +0.3$

average differences of 0.72 dex and 0.75 dex, respectively. This difference for the combination of W8498+W8542 and W8498+W8662 is determined to be 0.97 dex and 1.05 dex respectively.

Carbon abundances were derived for 25 potential CH star candidates using spectrum synthesis calculations of the C_2 band around 5165 Å. All 25 program stars exhibit enhanced carbon abundance with $[C/Fe]$ in the range $1.15 \leq [C/Fe] \leq 3.28$. We have compared our estimates of carbon abundance with that of high-resolution estimates whenever it is available. Comparisons with high-resolution estimates showed an average difference in carbon abundance ($[C/Fe]$) of 0.5 dex.

In this study, we identified potential CH star candidates and estimated their carbon abundances whenever possible. These stars exhibit enhanced carbon abundance and represent a confirmed sample of CEMP stars. While further detailed high-resolution spectroscopic analysis is needed to confirm sub-groups (CEMP-s, CEMP-r/s, or CEMP-r) to which these stars belong, this sample serves as crucial targets for future detailed chemical composition studies based on high-resolution spectroscopy. Such studies are expected to provide valuable insights into the early Galactic chemical evolution.

Table 5 Derived carbon abundances of the programme stars.

Star	$\log\epsilon(\text{C})$	$[\text{C}/\text{Fe}]$	$[\text{C}/\text{Fe}]$ (Lit.value)	Reference
HE 0002+0053	8.80	2.41	2.15	1
HE 0017+0055	8.95	1.64	2.17	2
HE 0037-0654	8.55	2.00	-	-
HE 0039-2635	8.55	2.94	2.32	3
HE 0155-2221	8.82	1.77	1.78	1
HE 0206-1916	8.55	2.83	-	-
HE 0228-0256	8.76	2.71	-	-
HE 0251-2118	8.67	1.16	1.13	1
HE 0258-0218	8.40	1.77	-	-
HE 0319-0215	8.55	3.21	-	-
HE 0322-1504	8.65	2.10	2.40	4
HE 0323-2702	8.58	1.77	-	-
HE 0507-1430	8.80	2.2	2.7	4
HE 0507-1653	8.50	1.71	1.30	5
HE 0518-2322	8.30	1.15	-	-
HE 1045-1434	8.70	3.28	-	-
HE 1157-0518	8.65	2.13	2.15	5
HE 1319-1935	8.55	2.79	-	-
HE 1429-0551	8.60	3.06	-	-
HE 1442-0346	8.43	1.96	-	-
HE 1523-1155	8.55	2.63	-	-
HE 2145-1715	8.41	2.64	1.14	1
HE 2150-1800	7.68	1.50	-	-
HE 2218+0127	8.63	1.87	-	-
HE 2339-0837	8.60	3.18	-	-

1. Kennedy et al (2011), 2. Jorissen et al (2016a), 3. Barbuy et al (1997), 4. Abate et al (2015), 5. Aoki et al (2007)

Acknowledgments. This work made use of the SIMBAD astronomical database, operated at CDS, Strasbourg, France, the NASA ADS, USA and data from the European Space Agency (ESA) mission Gaia (<https://www.cosmos.esa.int/gaia>), processed by the Gaia Data Processing and Analysis Consortium (DPAC, <https://www.cosmos.esa.int/web/gaia/dpac/consortium>). We thank the referee for many constructive suggestions and useful comments on the manuscript that improved this paper. We thank the staff at IAO, Hanle, and Centre For Research & Education in Science & Technology (CREST), Hoskote, for assistance during the observations. We extend our gratitude to Dr Drisya Karinkuzhi, Dr Shejeelammal J and Dr Partha Pratim Goswami for diligently observing several objects used for this study during their dedicated observing nights at CREST.

References

- Abate C, Pols OR, Izzard RG, et al (2015) Carbon-enhanced metal-poor stars: a window on AGB nucleosynthesis and binary evolution. II. Statistical analysis of a sample of 67 CEMP-s stars. *Astron. Astrophys.*581:A22. <https://doi.org/10.1051/0004-6361/201525876>, [arXiv:1507.04662](https://arxiv.org/abs/1507.04662) [astro-ph.SR]
- Abate C, Stancliffe RJ, Liu ZW (2016) How plausible are the proposed formation scenarios of CEMP-r/s stars? *Astron. Astrophys.*587:A50. <https://doi.org/10.1051/0004-6361/201527864>, [arXiv:1601.00976](https://arxiv.org/abs/1601.00976) [astro-ph.SR]

- Abbott BP, Abbott R, Abbott TD, et al (2017) Gravitational Waves and Gamma-Rays from a Binary Neutron Star Merger: GW170817 and GRB 170817A. *Astrophys. J. Lett.* 848(2):L13. <https://doi.org/10.3847/2041-8213/aa920c>, [arXiv:1710.05834](https://arxiv.org/abs/1710.05834) [astro-ph.HE]
- Adamczak J, Lambert DL (2014) Carbon and Oxygen Abundances across the Hertzsprung Gap. *Astrophys. J.* 791(1):58. <https://doi.org/10.1088/0004-637X/791/1/58>, [arXiv:1407.2157](https://arxiv.org/abs/1407.2157) [astro-ph.SR]
- Alonso A, Arribas S, Martínez-Roger C (1999) The effective temperature scale of giant stars (F0-K5). II. Empirical calibration of T_{eff} versus colours and [Fe/H]. *Astron. Astrophys. Suppl.* 140:261–277. <https://doi.org/10.1051/aas:1999521>
- Aoki W, Beers TC, Christlieb N, et al (2007) Carbon-enhanced Metal-poor Stars. I. Chemical Compositions of 26 Stars. *Astrophys. J.* 655(1):492–521. <https://doi.org/10.1086/509817>, [arXiv:astro-ph/0609702](https://arxiv.org/abs/astro-ph/0609702) [astro-ph]
- Arcones A, Thielemann FK (2013) Neutrino-driven wind simulations and nucleosynthesis of heavy elements. *Journal of Physics G Nuclear Physics* 40(1):013201. <https://doi.org/10.1088/0954-3899/40/1/013201>, [arXiv:1207.2527](https://arxiv.org/abs/1207.2527) [astro-ph.SR]
- Asplund M, Grevesse N, Sauval AJ, et al (2009) The Chemical Composition of the Sun. *Annu. Rev. Astron. Astrophys.* 47(1):481–522. <https://doi.org/10.1146/annurev.astro.46.060407.145222>, [arXiv:0909.0948](https://arxiv.org/abs/0909.0948) [astro-ph.SR]
- Barbuy B, Cayrel R, Spite M, et al (1997) Analysis of two CH/CN-strong very metal-poor stars. *Astron. Astrophys.* 317:L63–L66
- Barklem PS, Christlieb N, Beers TC, et al (2005) The Hamburg/ESO R-process enhanced star survey (HERES). II. Spectroscopic analysis of the survey sample. *Astron. Astrophys.* 439(1):129–151. <https://doi.org/10.1051/0004-6361:20052967>, [arXiv:astro-ph/0505050](https://arxiv.org/abs/astro-ph/0505050) [astro-ph]
- Barnbaum C, Stone RPS, Keenan PC (1996) A Moderate-Resolution Spectral Atlas of Carbon Stars: R, J, N, CH, and Barium Stars. *Astrophys. J. Suppl. Ser.* 105:419. <https://doi.org/10.1086/192323>
- Battistini C, Bensby T (2016) The origin and evolution of r- and s-process elements in the Milky Way stellar disk. *Astron. Astrophys.* 586:A49. <https://doi.org/10.1051/0004-6361/201527385>, [arXiv:1511.00966](https://arxiv.org/abs/1511.00966) [astro-ph.SR]
- Beers TC, Christlieb N (2005) The Discovery and Analysis of Very Metal-Poor Stars in the Galaxy. *Annu. Rev. Astron. Astrophys.* 43(1):531–580. <https://doi.org/10.1146/annurev.astro.42.053102.134057>
- Beers TC, Norris JE, Placco VM, et al (2014) Population Studies. XIII. A New Analysis of the Bidelman-MacConnell “Weak-metal” Stars—Confirmation of Metal-poor

- Stars in the Thick Disk of the Galaxy. *Astrophys. J.*794(1):58. <https://doi.org/10.1088/0004-637X/794/1/58>, [arXiv:1408.3165](https://arxiv.org/abs/1408.3165) [astro-ph.GA]
- Bidelman WP (1956) The carbon stars—An astrophysical enigma. *Vistas in Astronomy* 2(1):1428–1437. [https://doi.org/10.1016/0083-6656\(56\)90071-X](https://doi.org/10.1016/0083-6656(56)90071-X)
- Boeche C, Grebel EK (2016) SP_Ace: a new code to derive stellar parameters and elemental abundances. *Astron. Astrophys.*587:A2. <https://doi.org/10.1051/0004-6361/201526758>, [arXiv:1512.01546](https://arxiv.org/abs/1512.01546) [astro-ph.IM]
- Brewer JM, Fischer DA, Valenti JA, et al (2016) Spectral Properties of Cool Stars: Extended Abundance Analysis of 1,617 Planet-search Stars. *Astrophys. J. Suppl. Ser.*225(2):32. <https://doi.org/10.3847/0067-0049/225/2/32>, [arXiv:1606.07929](https://arxiv.org/abs/1606.07929) [astro-ph.SR]
- Carrera R, Gallart C, Pancino E, et al (2007) The Infrared Ca II Triplet as Metallicity Indicator. *Astron. J.*134(3):1298. <https://doi.org/10.1086/520803>, [arXiv:0705.3335](https://arxiv.org/abs/0705.3335) [astro-ph]
- Carrera R, Pancino E, Gallart C, et al (2013) The near-infrared Ca II triplet as a metallicity indicator - II. Extension to extremely metal-poor metallicity regimes. *Mon. Not. R. Astron. Soc.*434(2):1681–1691. <https://doi.org/10.1093/mnras/stt1126>, [arXiv:1306.3883](https://arxiv.org/abs/1306.3883) [astro-ph.GA]
- Cenarro AJ, Peletier RF, Sánchez-Blázquez P, et al (2007) Medium-resolution Isaac Newton Telescope library of empirical spectra - II. The stellar atmospheric parameters. *Mon. Not. R. Astron. Soc.*374(2):664–690. <https://doi.org/10.1111/j.1365-2966.2006.11196.x>, [arXiv:astro-ph/0611618](https://arxiv.org/abs/astro-ph/0611618) [astro-ph]
- Christlieb N, Green PJ, Wisotzki L, et al (2001) The stellar content of the Hamburg/ESO survey II. A large, homogeneously-selected sample of high latitude carbon stars. *Astron. Astrophys.*375:366–374. <https://doi.org/10.1051/0004-6361:20010814>, [arXiv:astro-ph/0106240](https://arxiv.org/abs/astro-ph/0106240) [astro-ph]
- da Silva R, Milone AdC, Rocha-Pinto HJ (2015) Homogeneous abundance analysis of FGK dwarf, subgiant, and giant stars with and without giant planets. *Astron. Astrophys.*580:A24. <https://doi.org/10.1051/0004-6361/201525770>
- Delgado Mena E, Tsantaki M, Adibekyan VZ, et al (2017) Chemical abundances of 1111 FGK stars from the HARPS GTO planet search program. II. Cu, Zn, Sr, Y, Zr, Ba, Ce, Nd, and Eu. *Astron. Astrophys.*606:A94. <https://doi.org/10.1051/0004-6361/201730535>, [arXiv:1705.04349](https://arxiv.org/abs/1705.04349) [astro-ph.SR]
- Drout MR, Piro AL, Shappee BJ, et al (2017) Light curves of the neutron star merger GW170817/SSS17a: Implications for r-process nucleosynthesis. *Science* 358(6370):1570–1574. <https://doi.org/10.1126/science.aag0049>, [arXiv:1710.05443](https://arxiv.org/abs/1710.05443) [astro-ph.HE]

- Frebel A, Christlieb N, Norris JE, et al (2006) Bright Metal-poor Stars from the Hamburg/ESO Survey. I. Selection and Follow-up Observations from 329 Fields. *Astrophys. J.* 652(2):1585–1603. <https://doi.org/10.1086/508506>, [arXiv:astro-ph/0608332](https://arxiv.org/abs/astro-ph/0608332) [astro-ph]
- Fulbright JP (2000) Abundances and Kinematics of Field Halo and Disk Stars. I. Observational Data and Abundance Analysis. *Astron. J.* 120(4):1841–1852. <https://doi.org/10.1086/301548>, [arXiv:astro-ph/0006260](https://arxiv.org/abs/astro-ph/0006260) [astro-ph]
- Gaia Collaboration, Prusti T, de Bruijne JHJ, et al (2016) The Gaia mission. *Astron. Astrophys.* 595:A1. <https://doi.org/10.1051/0004-6361/201629272>, [arXiv:1609.04153](https://arxiv.org/abs/1609.04153) [astro-ph.IM]
- Gaia Collaboration, Katz D, Antoja T, et al (2018) Gaia Data Release 2. Mapping the Milky Way disc kinematics. *Astron. Astrophys.* 616:A11. <https://doi.org/10.1051/0004-6361/201832865>, [arXiv:1804.09380](https://arxiv.org/abs/1804.09380) [astro-ph.GA]
- Gillon M, Magain P (2006) High precision determination of the atmospheric parameters and abundances of the COROT main targets. *Astron. Astrophys.* 448(1):341–350. <https://doi.org/10.1051/0004-6361:20053965>, [arXiv:astro-ph/0511099](https://arxiv.org/abs/astro-ph/0511099) [astro-ph]
- Girardi L, Bressan A, Bertelli G, et al (2000) Evolutionary tracks and isochrones for low- and intermediate-mass stars: From 0.15 to 7 M_{sun} , and from $Z=0.0004$ to 0.03. *Astron. Astrophys. Suppl.* 141:371–383. <https://doi.org/10.1051/aas:2000126>, [arXiv:astro-ph/9910164](https://arxiv.org/abs/astro-ph/9910164) [astro-ph]
- Goswami A (2005) CH stars at high Galactic latitudes. *Mon. Not. R. Astron. Soc.* 359(2):531–544. <https://doi.org/10.1111/j.1365-2966.2005.08917.x>, [arXiv:astro-ph/0507202](https://arxiv.org/abs/astro-ph/0507202) [astro-ph]
- Goswami A, Aoki W (2010) HD 209621: abundances of neutron-capture elements*. *Mon. Not. R. Astron. Soc.* 404(1):253–264. <https://doi.org/10.1111/j.1365-2966.2010.16265.x>, [arXiv:1002.4477](https://arxiv.org/abs/1002.4477) [astro-ph.SR]
- Goswami A, Prantzos N (2000) Abundance evolution of intermediate mass elements (C to Zn) in the Milky Way halo and disk. *Astron. Astrophys.* 359:191–212. <https://doi.org/10.48550/arXiv.astro-ph/0005179>, [arXiv:astro-ph/0005179](https://arxiv.org/abs/astro-ph/0005179) [astro-ph]
- Goswami A, Aoki W, Beers TC, et al (2006) A high-resolution spectral analysis of three carbon-enhanced metal-poor stars. *Mon. Not. R. Astron. Soc.* 372(1):343–356. <https://doi.org/10.1111/j.1365-2966.2006.10877.x>, [arXiv:astro-ph/0608106](https://arxiv.org/abs/astro-ph/0608106) [astro-ph]
- Goswami A, Bama P, Shantikumar NS, et al (2007) Low-resolution spectroscopy of high Galactic latitude objects: A search for CH stars. *Bulletin of the Astronomical Society of India* 35:339

- Goswami A, Karinkuzhi D, Shantikumar NS (2010) The CH fraction of carbon stars at high Galactic latitudes. *Mon. Not. R. Astron. Soc.*402(2):1111–1125. <https://doi.org/10.1111/j.1365-2966.2009.15939.x>, [arXiv:0912.4347](https://arxiv.org/abs/0912.4347) [astro-ph.SR]
- Goswami A, Aoki W, Karinkuzhi D (2016) Subaru/HDS study of CH stars: elemental abundances for stellar neutron-capture process studies. *Mon. Not. R. Astron. Soc.*455(1):402–422. <https://doi.org/10.1093/mnras/stv2011>, [arXiv:1510.07814](https://arxiv.org/abs/1510.07814) [astro-ph.SR]
- Goswami PP, Rathour RS, Goswami A (2021) Spectroscopic study of CEMP-(s & r/s) stars. Revisiting classification criteria and formation scenarios, highlighting i-process nucleosynthesis. *Astron. Astrophys.*649:A49. <https://doi.org/10.1051/0004-6361/202038258>, [arXiv:2101.09518](https://arxiv.org/abs/2101.09518) [astro-ph.SR]
- Hansen CJ, Nordström B, Hansen TT, et al (2016a) Abundances of carbon-enhanced metal-poor stars as constraints on their formation. *Astron. Astrophys.*588:A37. <https://doi.org/10.1051/0004-6361/201526895>, [arXiv:1511.07812](https://arxiv.org/abs/1511.07812) [astro-ph.SR]
- Hansen T, Andersen J, Nordström B, et al (2011) The Binary Frequency of r-Process-element-enhanced Metal-poor Stars and Its Implications: Chemical Tagging in the Primitive Halo of the Milky Way. *Astrophys. J. Lett.*743(1):L1. <https://doi.org/10.1088/2041-8205/743/1/L1>, [arXiv:1110.4536](https://arxiv.org/abs/1110.4536) [astro-ph.GA]
- Hansen TT, Andersen J, Nordström B, et al (2016b) The role of binaries in the enrichment of the early Galactic halo. III. Carbon-enhanced metal-poor stars - CEMP-s stars. *Astron. Astrophys.*588:A3. <https://doi.org/10.1051/0004-6361/201527409>, [arXiv:1601.03385](https://arxiv.org/abs/1601.03385) [astro-ph.SR]
- Hekker S, Meléndez J (2007) Precise radial velocities of giant stars. III. Spectroscopic stellar parameters. *Astron. Astrophys.*475(3):1003–1009. <https://doi.org/10.1051/0004-6361:20078233>, [arXiv:0709.1145](https://arxiv.org/abs/0709.1145) [astro-ph]
- Herwig F (2005) Evolution of Asymptotic Giant Branch Stars. *Annu. Rev. Astron. Astrophys.*43(1):435–479. <https://doi.org/10.1146/annurev.astro.43.072103.150600>
- Jofré E, Petrucci R, Saffe C, et al (2015) Stellar parameters and chemical abundances of 223 evolved stars with and without planets. *Astron. Astrophys.*574:A50. <https://doi.org/10.1051/0004-6361/201424474>, [arXiv:1410.6422](https://arxiv.org/abs/1410.6422) [astro-ph.EP]
- Jofré P, Heiter U, Soubiran C, et al (2014) Gaia FGK benchmark stars: Metallicity. *Astron. Astrophys.*564:A133. <https://doi.org/10.1051/0004-6361/201322440>, [arXiv:1309.1099](https://arxiv.org/abs/1309.1099) [astro-ph.GA]
- Johnson JA, Herwig F, Beers TC, et al (2007) A Search for Nitrogen-enhanced Metal-poor Stars. *Astrophys. J.*658(2):1203–1216. <https://doi.org/10.1086/510114>, [arXiv:astro-ph/0608666](https://arxiv.org/abs/astro-ph/0608666) [astro-ph]

- Jorissen A, Hansen T, Van Eck S, et al (2016a) HE 0017+0055: A probable pulsating CEMP-rs star and long-period binary. *Astron. Astrophys.*586:A159. <https://doi.org/10.1051/0004-6361/201526993>, [arXiv:1510.06045](https://arxiv.org/abs/1510.06045) [astro-ph.SR]
- Jorissen A, Hansen T, Van Eck S, et al (2016b) HE 0017+0055: A probable pulsating CEMP-rs star and long-period binary. *Astron. Astrophys.*586:A159. <https://doi.org/10.1051/0004-6361/201526993>, [arXiv:1510.06045](https://arxiv.org/abs/1510.06045) [astro-ph.SR]
- Karakas AI, Lattanzio JC (2014) The Dawes Review 2: Nucleosynthesis and Stellar Yields of Low- and Intermediate-Mass Single Stars. *Publ. Astron. Soc. Aust.*31:e030. <https://doi.org/10.1017/pasa.2014.21>, [arXiv:1405.0062](https://arxiv.org/abs/1405.0062) [astro-ph.SR]
- Karinkuzhi D, Goswami A (2014) Chemical analysis of CH stars - I. Atmospheric parameters and elemental abundances. *Mon. Not. R. Astron. Soc.*440(2):1095–1113. <https://doi.org/10.1093/mnras/stu148>, [arXiv:1410.0111](https://arxiv.org/abs/1410.0111) [astro-ph.SR]
- Karinkuzhi D, Goswami A (2015) Chemical analysis of CH stars - II. Atmospheric parameters and elemental abundances. *Mon. Not. R. Astron. Soc.*446(3):2348–2362. <https://doi.org/10.1093/mnras/stu2079>, [arXiv:1412.3548](https://arxiv.org/abs/1412.3548) [astro-ph.SR]
- Kennedy CR, Sivarani T, Beers TC, et al (2011) [O/Fe] Estimates for Carbon-enhanced Metal-poor Stars from Near-infrared Spectroscopy. *Astron. J.*141(3):102. <https://doi.org/10.1088/0004-6256/141/3/102>, [arXiv:1101.2260](https://arxiv.org/abs/1101.2260) [astro-ph.SR]
- Koleva M, Vazdekis A (2012) Stellar population models in the UV. I. Characterisation of the New Generation Stellar Library. *Astron. Astrophys.*538:A143. <https://doi.org/10.1051/0004-6361/201118065>, [arXiv:1111.5449](https://arxiv.org/abs/1111.5449) [astro-ph.CO]
- Lambert DL, Gustafsson B, Eriksson K, et al (1986) The Chemical Composition of Carbon Stars. I. Carbon, Nitrogen, and Oxygen in 30 Cool Carbon Stars in the Galactic Disk. *Astrophys. J. Suppl. Ser.*62:373. <https://doi.org/10.1086/191145>
- Liu YJ, Tan KF, Wang L, et al (2014) The Lithium Abundances of a Large Sample of Red Giants. *Astrophys. J.*785(2):94. <https://doi.org/10.1088/0004-637X/785/2/94>, [arXiv:1404.1687](https://arxiv.org/abs/1404.1687) [astro-ph.SR]
- Lucatello S, Tsangarides S, Beers TC, et al (2005) The Binary Frequency Among Carbon-enhanced, s-Process-rich, Metal-poor Stars. *Astrophys. J.*625(2):825–832. <https://doi.org/10.1086/428104>, [arXiv:astro-ph/0412422](https://arxiv.org/abs/astro-ph/0412422) [astro-ph]
- Lugaro M, Herwig F, Lattanzio JC, et al (2003) s-Process Nucleosynthesis in Asymptotic Giant Branch Stars: A Test for Stellar Evolution. *Astrophys. J.*586(2):1305–1319. <https://doi.org/10.1086/367887>, [arXiv:astro-ph/0212364](https://arxiv.org/abs/astro-ph/0212364) [astro-ph]
- Maldonado J, Eiroa C, Villaver E, et al (2012) Metallicity of solar-type stars with debris discs and planets*. *Astron. Astrophys.*541:A40. <https://doi.org/10.1051/0004-6361/201218800>, [arXiv:1202.5884](https://arxiv.org/abs/1202.5884) [astro-ph.EP]

- Massarotti A, Latham DW, Stefanik RP, et al (2008) Rotational and Radial Velocities for a Sample of 761 HIPPARCOS Giants and the Role of Binarity. *Astron. J.*135(1):209–231. <https://doi.org/10.1088/0004-6256/135/1/209>
- McClure RD, Woodsworth AW (1990) The Binary Nature of the Barium and CH Stars. III. Orbital Parameters. *Astrophys. J.*352:709. <https://doi.org/10.1086/168573>
- Mishenina TV, Soubiran C, Kovtyukh VV, et al (2012) Activity and the Li abundances in the FGK dwarfs*. *Astron. Astrophys.*547:A106. <https://doi.org/10.1051/0004-6361/201118412>, [arXiv:1210.6843](https://arxiv.org/abs/1210.6843) [astro-ph.SR]
- Montes D, González-Peinado R, Tabernero HM, et al (2018) Calibrating the metallicity of M dwarfs in wide physical binaries with F-, G-, and K-primaries - I: High-resolution spectroscopy with HERMES: stellar parameters, abundances, and kinematics. *Mon. Not. R. Astron. Soc.*479(1):1332–1382. <https://doi.org/10.1093/mnras/sty1295>, [arXiv:1805.05394](https://arxiv.org/abs/1805.05394) [astro-ph.SR]
- Pereira CB, Junqueira S (2003) Spectroscopic analysis of two CH subgiant stars: HD 50264 and HD 87080. *Astron. Astrophys.*402:1061–1071. <https://doi.org/10.1051/0004-6361:20030209>
- Placco VM, Beers TC, Ivans II, et al (2015) Hubble Space Telescope Near-Ultraviolet Spectroscopy of Bright CEMP-s Stars. *Astrophys. J.*812(2):109. <https://doi.org/10.1088/0004-637X/812/2/109>, [arXiv:1508.05872](https://arxiv.org/abs/1508.05872) [astro-ph.SR]
- Preston GW, Sneden C (2001) The Incidence of Binaries among Very Metal-poor Carbon Stars. *Astron. J.*122(3):1545–1560. <https://doi.org/10.1086/322082>
- Prugniel P, Vauglin I, Koleva M (2011) The atmospheric parameters and spectral interpolator for the MILES stars. *Astron. Astrophys.*531:A165. <https://doi.org/10.1051/0004-6361/201116769>, [arXiv:1104.4952](https://arxiv.org/abs/1104.4952) [astro-ph.CO]
- Purandardas M, Goswami A (2021a) Chemical Analysis of Two Extremely Metal-poor Stars HE 2148-2039 and HE 2155-2043. *Astrophys. J.*912(1):74. <https://doi.org/10.3847/1538-4357/abec45>, [arXiv:2103.07075](https://arxiv.org/abs/2103.07075) [astro-ph.SR]
- Purandardas M, Goswami A (2021b) Observational evidence points at AGB stars as possible progenitors of CEMP-s & r/s stars. *arXiv e-prints* [arXiv:2108.06075](https://arxiv.org/abs/2108.06075) [astro-ph.SR]
- Purandardas M, Goswami A, Goswami PP, et al (2019) Chemical analysis of CH stars - III. Atmospheric parameters and elemental abundances. *Mon. Not. R. Astron. Soc.*486(3):3266–3289. <https://doi.org/10.1093/mnras/stz759>, [arXiv:1904.03904](https://arxiv.org/abs/1904.03904) [astro-ph.SR]
- Ramírez I, Fish JR, Lambert DL, et al (2012) Lithium Abundances in nearby FGK Dwarf and Subgiant Stars: Internal Destruction, Galactic Chemical Evolution, and

- Exoplanets. *Astrophys. J.*756(1):46. <https://doi.org/10.1088/0004-637X/756/1/46>, [arXiv:1207.0499](https://arxiv.org/abs/1207.0499) [astro-ph.SR]
- Ramírez I, Allende Prieto C, Lambert DL (2013) Oxygen Abundances in Nearby FGK Stars and the Galactic Chemical Evolution of the Local Disk and Halo. *Astrophys. J.*764(1):78. <https://doi.org/10.1088/0004-637X/764/1/78>, [arXiv:1301.1582](https://arxiv.org/abs/1301.1582) [astro-ph.SR]
- Roriz MP, Pereira CB, Junqueira S, et al (2023) High-resolution spectroscopic analysis of four new chemically peculiar stars. *Mon. Not. R. Astron. Soc.*518(4):5414–5443. <https://doi.org/10.1093/mnras/stac3378>, [arXiv:2211.08627](https://arxiv.org/abs/2211.08627) [astro-ph.SR]
- Rosswog S, Korobkin O, Arcones A, et al (2014) The long-term evolution of neutron star merger remnants - I. The impact of r-process nucleosynthesis. *Mon. Not. R. Astron. Soc.*439(1):744–756. <https://doi.org/10.1093/mnras/stt2502>, [arXiv:1307.2939](https://arxiv.org/abs/1307.2939) [astro-ph.HE]
- Shappee BJ, Simon JD, Drout MR, et al (2017) Early spectra of the gravitational wave source GW170817: Evolution of a neutron star merger. *Science* 358(6370):1574–1578. <https://doi.org/10.1126/science.aag0186>, [arXiv:1710.05432](https://arxiv.org/abs/1710.05432) [astro-ph.HE]
- Smith VV, Coleman H, Lambert DL (1993) Abundances in CH Subgiants: Evidence of Mass Transfer onto Main-Sequence Companions. *Astrophys. J.*417:287. <https://doi.org/10.1086/173311>
- Snedden CA (1973) Carbon and Nitrogen Abundances in Metal-Poor Stars. PhD thesis, THE UNIVERSITY OF TEXAS AT AUSTIN.
- Soubiran C, Le Campion JF, Brouillet N, et al (2016) The PASTEL catalogue: 2016 version. *Astron. Astrophys.*591:A118. <https://doi.org/10.1051/0004-6361/201628497>, [arXiv:1605.07384](https://arxiv.org/abs/1605.07384) [astro-ph.SR]
- Yang GC, Liang YC, Spite M, et al (2016) Chemical abundance analysis of 19 barium stars. *Research in Astronomy and Astrophysics* 16(1):19. <https://doi.org/10.1088/1674-4527/16/1/019>, [arXiv:1602.08704](https://arxiv.org/abs/1602.08704) [astro-ph.SR]
- Yong D, Norris JE, Bessell MS, et al (2013) The Most Metal-poor Stars. II. Chemical Abundances of 190 Metal-poor Stars Including 10 New Stars with $[Fe/H]_j = -3.5$. *Astrophys. J.*762(1):26. <https://doi.org/10.1088/0004-637X/762/1/26>, [arXiv:1208.3003](https://arxiv.org/abs/1208.3003) [astro-ph.GA]
- Yoon J, Beers TC, Placco VM, et al (2016) Observational Constraints on First-star Nucleosynthesis. I. Evidence for Multiple Progenitors of CEMP-No Stars. *Astrophys. J.*833(1):20. <https://doi.org/10.3847/0004-637X/833/1/20>, [arXiv:1607.06336](https://arxiv.org/abs/1607.06336) [astro-ph.SR]
- Zamora O, Abia C, Plez B, et al (2009) The chemical composition of carbon stars.

The R-type stars. *Astron. Astrophys.* 508(2):909–922. <https://doi.org/10.1051/0004-6361/200912843>, [arXiv:0909.4222](https://arxiv.org/abs/0909.4222) [astro-ph.SR]

Appendix A

Table A1 Temperatures from photometry

star name	T_{eff} (J-K)	T_{eff} (-0.5) (J-H)	T_{eff} (-1.0) (J-H)	T_{eff} (-1.5) (J-H)	T_{eff} (-2.0) (J-H)	T_{eff} (-0.5) (V-K)	T_{eff} (-1.0) (v-k)	T_{eff} (-1.5) (V-K)	T_{eff} (-2.0) (V-K)	T_{eff} (H_{α})
HE 0002+0053	4070.13	4392.57	4409.57	4407.08	4385.19	4095.07	4081.52	4072.94	4069.28	4250
HE 0017+0055	4261.44	4462.02	4479.96	4477.8	4455.61	4105.98	4092.46	4083.94	4080.36	4500
HE 0037-0654	5458.60	5146.13	5174.46	5176.03	5150.80	5328.81	5326.75	5332.36	5345.71	-
HE 0039-2635	4911.71	5064.04	5091.02	5092.09	5067.23	4820.78	4808.88	4803.26	5100	-
HE 0429+0232	4375.27	4612.36	4632.42	4630.99	4608.13	4215.14	4201.89	4193.9	4191.12	4600
HE 0443-1847	4559.4	4735.79	4757.66	4756.88	4733.47	4270.62	4257.49	4249.78	4247.39	4300
HE 0503-2009	4678.27	4774.69	4797.14	4796.57	4772.99	4476.99	4464.29	4457.53	4456.63	4450
HE 0507-1653	4935.03	5077.52	5104.72	5105.86	5080.95	4854.93	4843.61	4838.67	4840.07	5200
HE 0039-2635	4911.71	5064.044	5091.02	5092.09	5067.23	4820.78	4808.88	4803.26	4803.89	5100
HE 0206-1916	4885.40	4967.59	4993.02	4993.53	4969.09	4706.30	4692.49	4684.68	4682.83	4650
HE 0113+0110	4307.89	4279.09	4294.58	4291.59	4270.19	4356.06	4343.12	4335.79	4334.03	-
HE 0155-2221	4266.03	4325.55	4341.65	4338.86	4317.26	3993.42	3979.57	-	-	4500
HE 0228-0256	3926.25	4204.16	4218.68	4215.36	4194.3	4102.14	4088.61	4080.07	4076.47	4200
HE 0237-0835	4487.1	4605.11	4625.07	4623.61	4600.78	4468.31	4455.6	4448.79	4447.83	-
HE 0251-2118	4655.01	4778.62	4801.13	4800.58	4776.98	4579.4	4566.91	4560.6	4560.44	4400
HE 0258-0218	4586.99	4509.73	4528.34	4526.41	4503.99	5058.64	5051.06	5050.39	5056.63	4800
HE 0319-0215	-	4615.99	4636.10	4634.70	4611.82	4529.61	4517.02	4510.49	4509.97	4700
HE 0322-1504	4370.36	4597.89	4617.74	4616.24	4593.45	4228.24	4215.03	4207.1	4204.42	4600
HE 0323-2702	4701.82	4705.19	4726.6	4701.82	4702.39	4917.14	4906.93	4903.25	4906.08	4500
HE 0326-2603	-	5183.58	5212.52	5214.33	5188.94	5148.05	5142.22	5143.56	5152.06	-
HE 0333-1819	4387.60	4572.81	4592.30	4590.68	4567.99	4293.84	4280.77	4273.16	4270.95	-
HE 0341-0314	4298.49	4576.37	4595.92	4594.32	4571.62	4230.76	4217.55	4209.64	4206.97	-
HE 0359-0141	4243.24	4402.35	4419.47	4417.03	4395.09	4112.59	4099.09	4090.6	4087.07	4450
HE 0417-0513	4326.86	4350.81	4367.24	4364.56	4342.86	4026.51	4012.76	4003.83	3999.65	4100
HE 0422-2518	4529.54	4810.32	4833.31	4832.93	4809.19	-	-	-	-	-
HE 0443-1847	4559.40	4735.79	4757.66	4756.88	4733.47	4270.62	4257.49	4249.78	4247.40	4300
HE 0503-2009	4678.27	4774.69	4797.14	4796.57	4772.99	4476.99	4464.29	4457.53	4456.63	4450
HE 0507-1430	4407.51	4472.15	4490.23	4488.12	4465.87	4312.81	4299.78	4292.25	4290.18	4600
HE 0507-1653	4935.03	5077.52	5104.72	5105.87	5080.95	4854.93	4843.61	4838.67	4840.07	5200
HE 0508-1604	4432.75	4605.11	4625.06	4623.61	4600.78	4569.11	4556.59	4550.25	4550.01	4650
HE 0516-2515	4062.07	4300.63	4316.39	4313.5	4296.01	3917.3	3903.19	-	-	-
HE 0518-1751	4589.77	4697.61	4718.91	4717.92	4694.69	4312.81	4299.78	4292.25	4290.18	4350
HE 0518-2322	4885.4	4963.31	4988.67	4989.15	4964.73	4825.93	4814.11	4808.59	4809.34	5100
HE 0519-2053	4623.51	4619.63	4639.79	4638.41	4615.52	4643.32	4628.52	4619.56	4616.39	4400
HE 0919+0200	4487.01	4619.63	4639.79	4638.41	4615.52	4439.58	4426.81	4419.87	4418.7	4250
HE 0926-0417	4731.7	4778.62	4801.13	4800.58	4776.98	4743.88	4730.68	4723.58	4722.53	4500
HE 0930-0945	4672.42	4682.53	4703.6	4702.54	4679.37	4654.83	4640.2	4631.45	4628.52	-
HE 0930-0018	4163.85	4353.99	4370.46	4367.8	4346.08	4001.55	3987.73	3978.67	3974.3	4400
HE 1008-0946	4473.93	4523.58	4542.38	4540.51	4518.04	4033	4019.27	4010.38	4006.25	-
HE 1023-1504	4062.07	4143.52	4157.27	4153.69	4132.90	4211.43	4198.17	4190.17	4187.36	-
HE 1032-1655	4484.39	4506.29	4524.84	4522.89	4500.5	-	-	-	-	-
HE 1045-1434	4564.8	4933.53	4958.42	4958.73	4934.44	4689.67	4675.59	4667.48	4665.28	4800
HE 1058-1300	4448.07	4597.89	4617.74	4616.24	4593.45	4399.63	4386.78	4379.66	4378.2	-
HE 1104-0957	-	4180.82	4195.04	4191.63	4170.67	3964.96	3951.02	-	-	-
HE 1112-2557	4540.34	4708.99	4730.46	4729.54	4706.25	4364.64	4351.72	4344.43	4342.73	-
HE 1130-1956	4655.01	4774.69	4797.14	4796.57	4772.99	4436.51	4423.74	4416.79	4415.59	-
HE 1150-2049	4589.77	4637.93	4658.36	4657.07	4634.09	4496.15	4483.49	4476.82	4476.06	-
HE 1150-2546	4660.79	4708.99	4730.46	4729.54	4706.25	4407.06	4394.23	4387.14	4385.74	-
HE 1152-0355	4050.00	4260.83	4276.08	4273.00	4251.69	4199.16	4185.87	4177.81	4174.91	-
HE 1157-0518	4921.67	4871.05	4894.97	4894.92	4870.92	4770.93	4758.18	4751.59	4751.13	4700
HE 1158-0708	4078.22	4004.33	4016.38	-	-	4547.94	4535.39	4528.94	4528.56	-
HE 1205-0417	3983.95	4046.81	4059.37	4055.42	4035.04	3747.61	3732.73	-	-	-
HE 1205-0521	4768.22	5109.28	5137.00	5138.35	5113.29	4483.35	4470.66	4463.92	4463.07	5000
HE 1205-0849	4367.91	4451.95	4469.75	4467.54	4445.39	4505.85	4493.21	4486.58	4485.88	4600
HE 1208-1247	4341.23	4369.97	4386.66	4384.07	4362.28	4410.05	4397.22	4390.14	4388.76	-
HE 1212-0323	4415.04	4458.66	4476.55	4474.38	4452.19	4395.19	4382.34	4375.19	4373.71	-
HE 1212-1414	4365.47	4431.96	4449.48	4447.18	4425.12	-	-	-	-	-

star name	T_{eff} (J-K)	T_{eff} (-0.5) (J-H)	T_{eff} (-1.0) (J-H)	T_{eff} (-1.5) (J-H)	T_{eff} (-2.0) (J-H)	T_{eff} (-0.5) (V-K)	T_{eff} (-1.0) (v-k)	T_{eff} (-1.5) (V-K)	T_{eff} (-2.0) (V-K)	T_{eff} (H_{α})
HE 1221-0651	4458.37	4451.95	4469.75	4467.54	4445.39	4566.55	4554.03	4547.67	4547.42	-
HE 1236-0337	4289.15	4447.18	4449.48	4289.15	4425.12	4219.49	4206.25	4198.28	4195.54	-
HE 1238-1714	4617.85	4743.52	4765.49	4764.76	4741.32	4505.04	4492.4	4485.76	4485.06	-
HE 1241-0337	4189.85	4382.86	4399.71	4397.19	4375.34	4046.67	4032.98	4024.16	4020.13	4000
HE 1247-2554	4343.64	4502.85	4521.35	4519.39	4497.01	-	-	-	-	-
HE 1251-2313	4830.66	4980.5	5006.14	5006.72	4982.23	4796.24	4783.92	4777.82	4777.91	-
HE 1255-2324	4660.79	4925.09	4949.85	4950.12	4925.87	4455.8	4443.06	4436.19	4435.15	-
HE 1305+0007	4687.06	4899.98	4924.35	4924.47	4900.34	4460.48	4440.91	4447.75	4439.89	-
HE 1308-1012	5010.14	5104.72	5132.36	5133.68	5108.64	5263.57	5260.11	5264.15	5275.7	-
HE 1318-1657	4551.21	4826.35	4849.58	4849.29	4825.48	4489.73	4477.06	4470.35	4469.55	-
HE 1318-2451	4543.05	4660.11	4680.86	4679.68	4656.61	4381.99	4369.11	4361.91	4360.33	-
HE 1319-1935	4678.00	4623.28	4643.49	4642.13	4619.22	4546.27	4533.71	4527.25	4526.85	-
HE 1319-2340	4632.05	4778.62	4801.13	4800.58	4800.58	4326.57	4313.57	4306.11	4306.11	-
HE 1336+0200	3739.45	3950.12	3961.53	-	-	3687.35	3672.08	-	-	-
HE 1345-2616	4392.55	4572.81	4592.3	4590.68	4567.99	-	-	-	-	-
HE 1354-2552	4397.52	4548.05	4567.18	4565.44	4542.87	4232.02	4218.81	4210.91	4208.25	-
HE 1406-2016	4623.51	4739.65	4761.57	4760.82	4737.39	4346.13	4333.18	4325.81	4323.97	-
HE 1429-0551	4609.4	5037.33	5063.87	5064.79	5040.04	4527.13	4514.54	4507.99	4507.46	4800
HE 1430+0227	4500.19	4708.99	4730.46	4729.54	4706.25	4486.53	4473.86	4467.13	4466.3	-
HE 1431-0245	4915.03	4663.83	4684.63	4683.47	4660.39	4736.91	4723.59	4716.37	4715.16	-
HE 1442-0346	4719.69	4875.16	4899.14	4899.12	4875.09	4757.87	4744.9	4738.07	4737.31	4950
HE 1523-1155	4768.20	4770.77	4793.16	4792.56	4769.00	4580.26	4567.77	4561.47	4561.32	5000
HE 1528-0409	4872.30	4916.69	4941.32	4941.53	4917.33	4648.11	4633.38	4624.51	4621.44	-
HE 2138-1616	4891.95	5068.53	5095.58	5096.68	5071.79	4493.54	4481.89	4475.19	4474.42	4600
HE 2145-1715	4341.23	4254.78	4269.95	4266.85	4245.57	4233.91	4220.71	4212.82	4210.17	4100
HE 2150-1800	5017.11	5095.62	5123.11	5124.37	5099.37	4976.52	4967.40	4964.96	4969.20	4900
HE 2218+0127	5623.27	5785.56	5825.33	-	-	4505.04	4492.4	4485.76	4485.06	5400
HE 2224-0330	4968.82	5068.53	5095.58	5096.68	5071.79	4805.42	4793.25	4787.33	4787.62	4750
HE 2331-1329	-	3792.69	3802.31	-	-	3802.71	3788.13	-	-	-
HE 2339-0837	4830.7	4774.69	4797.14	4796.57	4772.99	5092.67	5085.75	5085.84	5092.93	4600
HE 2352-1906	4672.42	4834.41	4857.76	4857.51	4833.67	4516.44	4503.83	4497.24	4496.62	4450

The numbers in the parenthesis below T_{eff} indicate the metallicity values at which the temperatures are calculated. Temperatures are given in Kelvin.

Appendix B

Table B2 Metallicity from CaT lines for stars used for our analysis compared with literature high-resolution spectroscopic [Fe/H] estimates

Star name	V	Parallax(mas)	Mv	W8498	W8542	W8662	[Fe/H] (W8498+W8542+W8662)	[Fe/H] (W8498+W8542)	[Fe/H] (W8542+W8662)	[Fe/H] (W8498+W8662)	lit.value	reference
HD 4395	7.68	11.14±0.05	2.91	1.22	2.53	2.39	-0.16	-1.31	-0.74	-1.38	-0.27	1
											-0.38	2
											-0.16	3
HD 5395	4.62	17.28±0.19	0.81	0.69	2.15	1.6	-1.48	-2.22	-1.79	-2.49	-0.4	4
											-0.51	5
											-0.45	6
											-0.35	7
											-0.24	3
HD 16458	5.78	6.8±0.07	-0.06	0.85	2.46	2.21	-1.24	-2.19	-1.6	-2.31	-0.35	2
											-0.65	3
HD 22049	3.73	312.2±0.16	6.2	1.13	2.82	2.58	0.96	-0.44	0.35	-0.57	-0.15	8
											-0.09	9
HD 35410	5.07	16.7±0.16	1.18	1.29	2.83	2.59	-0.39	-1.54	-0.95	-1.65	-0.33	6
HD 43587	5.7	51.8±0.11	4.27	1.16	2.47	2.07	-0.005	-1.06	-0.59	-1.27	-0.28	2
											-0.12	1
											-0.03	10
											0.02	11
HD 48565	7.18	20.15±0.09	3.7	0.81	1.96	1.49	-0.87	-1.64	-1.28	-1.9	-0.63	4
											-0.59	3
											-0.7	12
HD 49738	5.67	2.85±0.09	-2.05	2.04	4.49	3.8	0.037	-1.38	-0.73	-1.65	-0.05	13
HD 55496	8.4	1.99±0.04	-0.097	0.67	2.05	2.44	-1.4	-2.47	-1.69	-2.29	-1.49	14
											-1.55	12
HD 89668	9.41	31.17±0.06	6.87	0.83	2.31	2.02	0.39	-0.75	-0.07	-0.92	-0.13	14
HD 90508	6.43	43.65±0.43	4.63	1.27	2.81	2.61	0.59	-0.74	-0.05	-0.85	-0.28	15
											-0.37	16
HD 104979	4.12	19.98±0.22	0.62	1.49	3.41	2.72	-0.16	-1.33	-0.79	-1.63	-0.26	14
											-0.35	17
											-0.51	5
											-0.45	6
HD 107574	8.54	7.47±0.06	2.9	0.66	1.72	1.73	-1.14	-2.02	-1.46	-2.01	-0.65	14
HD 111395	6.29	58.48±0.05	5.12	1.06	2.52	1.98	0.15	-0.89	-0.4	-1.19	0.1	18
											0.22	19
HD 111721	7.97	5.08±0.06	1.5	1.24	3.11	2.31	-0.32	-1.36	-0.87	-1.73	-1.11	14
											-1.39	20
											-1.54	21
HD 125079	8.63	3.38±0.06	1.27	1	2.82	2.42	-0.57	-1.65	-1.01	-1.84	-0.16	22
											-0.18	3
HD 126681	9.53	17.78±0.07	5.78	0.66	2.07	1.66	-0.3	-1.22	-0.66	-1.47	-0.9	14
											-1.3	23
HD 148897	5.24	48.7±0.13	-1.32	1.28	3.36	2.85	-0.8	-1.93	-1.3	-2.13	-1.02	3
											-0.5	2
HD 167768	6.0	9.29±0.09	0.84	1.2	3.05	2.46	-0.49	-1.56	-1.01	-1.83	-0.51	14
											-0.77	13
											-0.67	12
HD 188650	5.78	2.65±0.05	-2.1	1.09	2.61	2.24	-1.63	-2.49	-2.04	-2.64	-0.87	24
											-0.67	6
											-0.4	12
											-0.46	3
HD 201626	8.16	4.51±0.06	1.43	0.64	1.79	1.55	-1.54	-2.29	-1.84	-2.43	-2.1	25
											-1.5	26
											-1.39	3
HD 203638	5.36	12.91±0.15	0.91	0.96	2.97	2.58	-0.55	-1.69	-0.97	-1.87	0.27	27
											0.17	4
HD 204613	8.22	15.9±0.29	4.23	0.85	1.35	1.79	-0.88	-1.86	-1.33	-1.6	-0.24	14
											-0.51	12
											-0.32	28
HD 212943	4.8	21±0.24	1.41	1.09	2.74	2.18	-0.63	-1.62	-1.12	-1.88	-0.45	1
											-0.2	17
HD 216219	7.44	9.88±0.05	2.41	0.96	2.45	2.2	-0.55	-1.59	-0.99	-1.72	-0.4	1
											-0.36	4
											-0.17	3
HE 0106-0136	11.77	2.98±0.06	4.15	0.34	0.75	0.47	-2.31	-2.76	-2.6	-3.08	-1.85	29
HE 0117-0201	12.65	0.26±0.06	-0.25	0.33	0.47	0.39	-3.63	-4.21	-4.07	-4.38	-2.63	29
HE 0110-0406	12.48	0.65±0.07	1.56	0.86	1.04	1.01	-0.47	-1.25	-1.04	-1.3	30	
HE 0315-1749	10.18	6.60±0.03	4.28	0.24	0.48	0.36	-2.75	-3.35	-3.11	-3.64	-2.39	29
HE 0852-0139	10.8	9.07±0.04	5.58	1.1	1.98	1.38	0.27	-0.54	-0.66	-0.96	-1.03	29
HE 0920-0506	10.95	2.37±0.06	2.83	0.26	1.13	1	-2.63	-3.21	-2.82	-3.38	-1.01	29
HE 0959-1714	12.29	0.47±0.04	0.67	0.37	0.75	0.52	-3.05	-3.5	-3.32	-3.78	-2.37	29
HE 1008-0938	9.98	7.65±0.08	4.39	0.69	1.7	1.45	-1.33	-1.91	-1.61	-2.2	-1.01	29
HE 1119-0218	11.42	2.39±0.04	3.32	0.48	0.96	0.82	-2.21	-2.7	-2.51	-2.85	-1.67	29
HE 1304-0651	10.85	2.06±0.05	2.42	0.3	0.73	0.63	-2.61	-3.2	-2.84	-3.23	-2.19	29
HE 1316-1236	10.3	2.88±0.04	2.6	0.39	0.96	0.62	-2.44	-2.83	-2.67	-3.35	-1.41	29
HE 1348-0135	12.4	0.58±0.05	1.24	0.27	0.56	0.55	-3.15	-3.63	-3.45	-4.03	-2.61	29
HE 1442-0848	10.31	4.41±0.10	3.53	0.36	0.78	0.69	-2.71	-3.15	-3.14	-3.48	-0.95	29
HE 1521-0138	11.15	1.64±0.04	2.23	0.49	0.99	0.81	-2.39	-2.96	-2.64	-3	-1.59	29
HE 2137-1240	11.14	0.18±0.10	-2.56	0.39	0.73	0.58	-3.51	-3.94	-3.76	-4.09	-2.99	29
HE 2144-1832	10.97	0.42±0.04	-0.92	1.11	1.59	1.5	-0.96	-1.73	-1.66	-2.24	-1.7	31
HE 2349-1709	9.81	14.66±0.07	5.64	0.84	1.96	1.58	-1.05	-1.71	-1.41	-1.88	-1.06	29
HE 2320-0313	10.66	6.45±0.03	4.71	0.75	1.81	1.48	-1.26	-1.89	-1.58	-2.12	-1.03	29

1. Boeche and Grebel (2016), 2. Soubiran et al (2016), 3. Karinkuzhi and Goswami (2014), 4. Prugniel et al (2011), 5. Massarotti et al (2008), 6. Liu et al (2014), 7. Jofré et al (2015), 8. Delgado Mena et al (2017), 9. Jofré et al (2014), 10. Montes et al (2018), 11. Gillon and Magain (2006), 12. Cénarro et al (2007), 13. Hekker and Meléndez (2007), 14. Karinkuzhi and Goswami (2015), 15. Brewer et al (2016), 16. Ramírez et al (2013), 17. da Silva et al (2015), 18. Mishenina et al (2012), 19. Maldonado et al (2012), 20. Beers et al (2014), 21. Fulbright (2000), 22. Smith et al (1993), 23. Battistini and Bensby (2016), 24. Adamczak and Lambert (2014), 25. Abate et al (2015), 26. Placco et al (2015), 27. Koleva and Vazdekis (2012), 28. Ramírez et al (2012), 29. Frebel et al (2006), 30. Purandardas et al (2019), 31. Hansen et al (2016a)